Draft version July 9, 2009
Preprint typeset using LaTeX style emulateapj v. 04/20/08

arXiv:0907.1408v1 [astro-ph.GA] 9 Jul 2009

JOINT ANALYSIS OF NEAR-INFRARED PROPERTIES AND SURFACE BRIGHTNESS FLUCTUATIONS OF LMC STAR CLUSTERS

G. Raimondo[1]

Draft version July 9, 2009

ABSTRACT

Surface brightness fluctuations have been proved to be a very powerful technique to determine the distance and characterize the stellar content in extragalactic systems. Nevertheless, before facing the problem of stellar content in distant galaxies, we need to calibrate the method onto nearby well-known systems. In this paper we analyze the properties at J and K_s bands of a sample of 19 star clusters in the Large Magellanic Cloud (LMC), for which accurate near-infrared (NIR) resolved star photometry, and integrated photometry are available. For the same sample, we derive the SBF measurements in J and K_s-bands. We use the multi-purpose stellar population code *SPoT (Stellar POpulations Tools)* to simulate the color-magnitude diagram, stellar counts, integrated magnitudes, colors, and surface brightness fluctuations of each cluster. The present procedure allows us to estimate the age and metallicity of the clusters in a consistent way, and provides a new calibration of the empirical s-parameter. We take advantage of the high sensitivity of NIR surface brightness fluctuations to thermally pulsing asymptotic (TP-AGB) stars to test different mass-loss rates affecting the evolution of such stars. We argue that NIR-SBFs can contribute to the disentangling of the observable properties of TP-AGB stars, especially in galaxies, where a large number of these stars are present.

Subject headings: stars: AGB and post-AGB — stars: carbon — stars: mass loss — galaxies: stellar content — (galaxies:) Magellanic Clouds — galaxies: star clusters

1. INTRODUCTION

In the study of galaxies, the age and chemical composition of the stellar components are perhaps two of the major quantities to determine. Only then, we can trace the star formation, the chemical enrichment and the assembly history of galaxies (see, e.g. Renzini 2006). Since first applications, surface brightness fluctuations (SBFs) have been recognized to be effective to disentangle the evolutionary status of unresolved stellar populations in extragalactic systems (e.g. Tonry et al. 1990; Blakeslee et al. 2001; Liu et al. 2002; Cantiello et al. 2003; Jensen et al. 2003; Cantiello et al. 2005). SBFs are indeed much more sensitive to the brightest stars in the population in a given passband than integrated luminosities (e.g. Liu et al. 2000), since they are defined as the ratio of the second to the first moment of the stellar luminosity function (Tonry & Schneider 1988). Thus, for instance near-infrared (NIR) SBFs may be efficiently used to detect the presence of intermediate-age stellar populations whose light is dominated by asymptotic giant branch (AGB) stars (e.g. Frogel et al. 1990). Hence, it is now available an additional tool to supply information on stellar systems other than the classical age/metallicity indicators based on integrated light, as broadband colors, and spectral features (e.g. Worthey 1993; Bressan et al. 1994; Maraston 1998).

Several works have been conducted to investigate the influence of AGB stars on integrated colors and spectral features in both metal-rich and metal-poor stellar populations (e.g. Girardi & Bertelli 1998; Maraston 1998; Brocato et al. 1999a; Mouhcine & Lançon 2002; Bruzual & Charlot 2003; Maraston 2005; Fagiolini et al. 2007), while only a few have been devoted to SBFs. Attempts to understand how SBFs depend on the evolution parameters of AGB stars have been made, in the optical and NIR bands, by Liu et al. (2000), Cantiello et al. (2003), and Raimondo et al. (2005a) following different approaches. Liu and coworkers explored the effects of changing, by an arbitrary factor, the lifetimes of post-Main Sequence (MS) stars in stellar populations older than 1 Gyr, whereas Cantiello et al. (2003) and Raimondo et al. (2005a) linked the lifetime of AGB and thermally pulsing AGB (TP-AGB) stars, in the age range $0.1 \lesssim t(Gyr) \leq 14$, to mass-loss process, the poor knowledge of which is among major uncertainties in modeling AGB stars. These stars may expel material at rates up to 10^{-4} $M_{\odot}yr^{-1}$, eventually ejecting between 20 and 80 per cent of their initial MS mass. Thus, their lifetime and the efficiency of the third dredge-up (TDU), which drives the formation of AGB Carbon-rich (C-type) stars, may be drastically reduced. Raimondo et al. (2005a) found that number variations of TP-AGB stars marginally affect optical SBF magnitudes for populations older than $\sim$ 1 Gyr, and, in general, less than $\sim$0.5 mag in the NIR, confirming the reliability of the SBF method to measure distances to spheroids (Tonry et al. 2001). In the case of young/intermediate-age populations, instead, SBFs appear to be highly dependent on the adopted mass-loss scenario, i.e. the number of TP-AGB stars (Raimondo et al. 2005a). An important caveat must be then understood when using SBFs to measure distances to galaxies suspected to host intermediate-age populations.

The high sensitivity of NIR-SBFs to the evolutionary properties of AGB stars might be used, in turn, to test the prescriptions adopted in stellar models to describe the physical processes at work in such stars.

---

[1] INAF-Osservatorio Astronomico di Teramo, Via M. Maggini s.n.c., I-64100 Teramo, Italy; raimondo@oa-teramo.inaf.it

Big efforts to model stars beyond the core-helium burning phase have been recently conducted by several authors (e.g. Kitsikis & Weiss 2007; Marigo & Girardi 2007; Cristallo et al. 2008; Herwig 2008), however, so far, a complete understanding of all aspects of the physics and numerical methods which properly describe AGB evolution is missing. As a matter of fact, the complex interplay between pulsation and mass-loss process, their dependence on metallicity and stellar mass, and interior nucleosynthesis coupled with envelope chemical enrichment are the major sources of uncertainty in predicting broad-band colors, abundances and luminosity of intermediate-age stellar populations. Therefore, whatever the technique to derive the evolutionary status of the population is, consistency checks between model predictions and observations for nearby resolved populations are still a prime step.

In a previous paper (Raimondo et al. 2005a) we measured optical-SBF amplitudes of 11 clusters in the Large Magellanic Cloud (LMC) using data from the Wide-Field Planetary Camera 2 (WFPC2) onboard *Hubble Space Telescope (HST)*. In that work, we showed that the SBF data/model comparison suffers of a large uncertainty when a cluster contains a small number of stars evolved off the MS, especially giant stars. Thus, we suggested that a different algorithm has to be used to predict SBF amplitudes for star clusters, due to the paucity of stars in such systems. González et al. (2004) used a different approach: they built up 8 super-clusters by coadding clusters in the LMC and the Small Magellanic Cloud (SMC) having the same Searle et al. (1980, SWB) class. The authors measured NIR-SBFs of these super-clusters using the Second Incremental and All Sky Data releases of the Two-Micron All Sky Survey (2MASS). To some extent, grouping clusters reduces stochastic effects due to small numbers of stars on fast evolutionary phases, however, this procedure suffers of the uncertainty in defining the membership of the cluster to the SWB classes as well as of the uncertainty of the relationship between the s-parameter and the cluster age. Moreover, Mouhcine et al. (2005) and Raimondo et al. (2005a) argued that the discrepancy between predicted and observed SBFs of some super-clusters is likely due to observational reasons, as contamination by foreground sources, and low-quality photometry of stars in the central, most crowded, regions. Therefore, obtaining new SBF measures from NIR data having better spatial resolution and sky stability is a necessary step toward constraining more tightly stellar population models.

In this paper we analyze the properties of a sample of nearby populous intermediate-age stellar clusters expected to host TP-AGB stars. We study 19 star clusters of LMC observed in the NIR by Ferraro et al. (2004) and Mucciarelli et al. (2006), and analyze their color-magnitude diagram (CMD), luminosity functions (LFs), integrated colors, magnitudes, and SBF amplitudes. From resolved-star photometry and total fluxes we measure SBFs in the J and K_s pass-bands. The multi-purpose stellar population synthesis code *SPoT* (Stellar Population Tools[2], Raimondo et al. 2005a) is used to derive theoretical SBF amplitudes, CMDs, integrated magnitudes, and colors of each cluster. We explore the sensitivity of SBFs to TP-AGB stars by changing the mass-loss rates. In the models presented here, the mass-loss rate is assumed to be the main parameter triggering the lifetime of TP-AGB stars, whereas the other relevant physical quantities quoted above are assumed to be similar in each models. The goal of the present paper is then twofold. First, we intend to reproduce the cluster's CMD, LFs, colors, and SBFs by means of a unique theoretical framework. Second, we address whether a connection between SBFs and TP-AGB star properties (number) and cluster age can be discerned in SBF data. The paper is organized as follows. § 2 details ingredients of the stellar population synthesis (SPS) code, including a brief description of the method adopted to derive integrated quantities (colors and SBFs). In § 3, we present the cluster sample and data, and in § 4 we compare synthetic CMDs, LFs, integrated colors, magnitudes and SBFs to the corresponding observed quantities. The final section provides a summary and discussion of our results.

2. STELLAR POPULATION SYNTHESIS CODE

The SPS models presented in this paper are based on an updated version of the stellar population synthesis code *SPoT*, designed to reproduce the properties of both resolved and unresolved stellar populations. SPS model predictions were applied and tested on star clusters of the Galaxy and MCs in previous papers (e.g. Brocato et al. 1999a, 2000, 2003; Raimondo et al. 2002, 2005a; Cantiello et al. 2003, 2007). In this section, we briefly describe the main ingredients, techniques to derive integrated quantities, and outline changes. We refer the reader to the cited papers for more details.

Differently from most SPS codes that are based on isochrones, the *SPoT* code directly relies on stellar evolutionary tracks. The present version utilizes the updated evolution stellar library by Pietrinferni et al. (2004)[3] for masses $0.5 \leq M/M_{\odot} \leq 11$. The stellar models cover all the evolutionary phases from MS up to carbon ignition or the onset of thermal pulses (TPs). This allows us to analyze stellar populations in the age range from ≈ 50 Myr to 14 Gyr. Stars of mass $0.1 \lesssim M/M_{\odot} < 0.5$ are from Brocato et al. (1998). Masses lower than this limit (central H-ignition, $M \approx 0.08\,M_{\odot}$) do not significantly contribute to the total mass of the cluster (see e.g. Chabrier & Mera 1997), and so they are not taken into account.

The mass of each star is randomly generated by using Monte Carlo techniques, while the mass distribution is shaped by the Initial Mass Function (IMF) from Kroupa (2001). The evolutionary line of each mass is then calculated by interpolating the available tracks in the mass grid.

2.1. *Horizontal Branch, AGB and TP-AGB stars*

The code is suited to simulate the color distribution of He-burning stars on the horizontal branch (HB) as a function of age, metallicity and mass-loss rate in old stellar populations ($t \gtrsim 5$ Gyr; e.g. Brocato et al. 1999b; Raimondo et al. 2002). The mass loss suffered by RGB stars is evaluated according to the Reimers formulation, where the Reimers' parameter η_i^R (i refers to the i-th RGB star) follows a Gaussian distribution-function with a mean value $\langle\eta^R\rangle = 0.4$ in our *standard models.* Thus, a generic RGB star losses mass at rate:

---

[2] http://www.oa-teramo.inaf.it/SPoT

[3] The stellar evolutionary library by Pietrinferni et al. (2004) (BaSTI web-site: http://www.oa-teramo.inaf.it/BaSTi) have been recently recomputed by the authors.

$$\dot{M}_i^R = -4 \cdot 10^{-13} \eta_i^R \cdot L_i R_i / M_i, \tag{1}$$

where L_i, R_i, M_i are respectively the star luminosity, radius and total mass in solar units. The result of this procedure is that He-burning stars are spread on the HB as observed in Galactic globular clusters (e.g. Brocato et al. 2000; Raimondo et al. 2002). SBF amplitudes of stellar populations older than ~ 5 Gyr were linked to the HB morphology as a function of η^R in Cantiello et al. (2003).

The evolution of stars off the zero-age HB till the double-shell phase is followed by interpolating the evolutionary tracks of Pietrinferni et al. (2004). In the case of intermediate-age populations, the stellar mass evolving off the turn-off (TO) point is high enough to prevent the RGB phase (i.e. no degenerate He core is developed), so that mass loss does not affect sizeably the color distribution of He-burning stars.

Beyond the early-AGB phase, stars with a MS mass in the range $M \sim 1 - 8$ $M_\odot$ (the upper limit, called M_{up}, depends on metallicity) undergo the TP-AGB phase. TP-AGB synthetic models (e.g. Renzini & Voli 1981; Iben & Renzini 1983) and hybrid models, which combine aspects of synthetic and full evolution (e.g. Marigo 1998), were developed with the aim to supply simplified descriptions of stellar evolution in this phase, using recipes and descriptions based on full evolutionary models and/or derived from empirical calibrations. In our code a specific routine evaluates the properties of expected TP-AGB stars by integrating the analytic formulas of Wagenhuber & Groenewegen (1998, hereandafter WG98), as described in Raimondo et al. (2005a, see Appendix A). It calculates the time evolution of the stellar core mass and luminosity, the starting point being the helium-core mass, luminosity, and temperature at the first thermal pulse. The WG98 description includes three important effects: (*i*) the first pulses do not reach the full amplitude; (*ii*) the hot bottom burning process that occurs in massive stars; and (*iii*) the TDU, even though this last phenomenon is treated in a simple way. In fact, in their models WG98 assumed that there is dredge-up only if the core mass is higher than a critical value and that the free parameter λ, describing the dredge-up efficiency, is constant. The limit of this formulation is that these descriptions and formulae do not account for the influence of abundance changes and nucleosynthesis in general on the evolution of the star. In the present work, the effective temperature (T_{eff}) is evaluated using relations of Wood (1990, hereafter W90), slightly shifted ($\Delta \log T_{eff} = -0.05$) to match present evolutionary tracks.

All stars are oxygen-rich (O-rich) when they enter the AGB phase. Whether or not they become C-rich stars primarily depends on the efficiency of the TDU occurring in the TP-AGB phase and on the extent and time-variation of the mass loss (e.g. Straniero et al. 1997). However, several effects play a role. In low-metallicity stars ($Z < 0.004$), the amount of oxygen in the envelope is so low that a few thermal pulses are sufficient to convert an O-rich star into a C-star (Renzini & Voli 1981). Moreover, the lower the metallicity the lower the minimum mass for the onset of TDU (e.g. Straniero et al. 2003). On the other hand, strong mass-loss episodes in TP-AGB stars may delay or even prevent the TDU occurrence and the formation of C-rich low-mass stars (Marigo et al. 1999). To introduce the metallicity dependence of the O- to C-star ratio, we consider the relation empirically derived in galaxies of the Local Group by Groenewegen (2007). So that, we assume that the ratio of the duration of the two sub-phases for each star with a given metallicity is constant.

Finally, post-AGB evolution experienced by stars before entering the white dwarf cooling sequence has a negligible impact in simulating the NIR properties of individual clusters, thus in the present work, such kind of stars are not considered.

2.2. *Mass loss of TP-AGB stars*

Major uncertainties in modeling the TP-AGB phase are related to the duration of this phase and to variations of stellar luminosity and chemistry. As already stated, the duration is highly triggered by various physical mechanisms, and primarily driven by the efficiency of mass-loss processes. To account for current uncertainties in the mass-loss rate determinations, we consider four different mass-loss prescriptions, and assume that the other relevant physical quantities are described by the WG98 and W90 formulations. Our aim is to investigate *if and how* they produce sizable effects on the foreseen observational quantities, SBFs in particular. Our final goal is to test the sensitivity of SBFs to the number of TP-AGB stars, and to investigate whether SBF predictions/data of well studied MCs star clusters may give suggestions about the number of TP-AGB stars.

In Raimondo et al. (2005a) we adopted the mass-loss rate formulation of Bloecker (1995) based on the dynamical theoretical investigation on the atmospheres of Mira-like variables by Bowen (1988) and valid for long period variable (LPV) stars with periods $P > 100$ days:

$$\dot{M}^{B95} = 4.83 \cdot 10^{-9} \eta^B M^{-2.1} L^{2.7} \dot{M}^R \tag{2}$$

where the index i is suppressed for simplicity; M is the MS mass, η^B is a scaling factor, equal to unity in Raimondo et al. (2005a), and $\dot{M}^R$ is the Reimers mass-loss rate with $\eta^R = 1$.

The four models considered in the present paper are defined by the following mass-loss laws:

− *Model A*: The mass-loss rate of Bloecker (1995, Eq. 2) with $\eta^B = 0.01$ and $\eta^B = 0.05$ is applied to stars with $M \geq 1.2 M_\odot$, whereas for lower masses the improved description for cool winds of tip-AGB stars by Wachter et al. (2002) is adopted:

$$\dot{M}^{W02} = -4.52 - 6.81 \log(T_{eff}/2600) + 2.47 \log(L/10^4 L_\odot) - 1.95 \log(\tag{3}$$

− *Model B*: The original Bloecker's law with $\eta^B = 1$ is applied to the full range of masses.

− *Model C*: The empirical mass-loss rate derived by van Loon et al. (2005) for O-rich dust-enshrouded AGB stars in the LMC is assumed. Through the modeling of spectral energy distributions, the authors estimated a mass-loss rate as a function of stellar luminosity and effective temperature:

$$\log \dot{M}^{V05} = -5.65+1.05\log(L/10000L_{\odot})-6.3\log(T_{eff}/3500K) \tag{4}$$

− *Model D*: The law proposed by van Loon (2007) for very bright stars with dust-driven mass-loss is adopted

$$\dot{M}^{V06} = 1.5\times10^{-9} Z[Z_{\odot}]^{-0.5}\, L[L_{\odot}]^{0.75}\, A_V^{0.75} \tag{5}$$

Here, A_V is the visual extinction ranging from about 0.01 up to 100 (van Loon 2007). In our synthesis models we assumed A_V as a free parameter, and find *a posteriori* that values in the range 0.01−1 are suitable to reproduce present NIR data. This is because most dust-enshrouded AGB stars are visible at longer wavelengths compared to the ones used here (J and K_s bands). Moreover, from the analysis of a sample of oxygen-rich AGB stars, Heras & Hony (2005) determined a mass-loss rate in the range $5\times10^{-8}\div10^{-5}$ $M_{\odot}$ yr^{-1} and a visual optical depth of $0.03\div0.6$ for stars with a small amount of dust in their envelopes.

To illustrate differences between models, we computed the mass-loss rate evolution of three TP-AGB stars of $M = 1.4$, 2.8, and 4.6 $M_{\odot}$ at fixed metallicity ($Z = 0.008$). The resulting evolutionary paths as a function of the pulsation period are reported in Figure 1. Theoretical fundamental periods were calculated from period-mass-luminosity relations for long period variables of Fox & Wood (1982), as reported by Marigo & Girardi (2007), under the assumption that stars pulsate everywhere on the TP-AGB phase, even if an instability strip should be considered (Groenewegen & de Jong 1994). Theoretical sequences are qualitatively compared with empirical mass-loss rates, derived from IR fluxes and CO radio line emission, and pulsation periods from observed light curves of a sample of obscured C- and O-rich stars (Whitelock et al. 2003) and C-stars (Groenewegen et al. 2007) in LMC. In the figure Galactic AGB stars observed by Whitelock et al. (2006), Winters et al. (2003), and Schöier & Olofsson (2001) are also plotted. As remarked by Whitelock et al. (2006), the two populations do not show remarkably differences in color and period relations. A similar conclusion can be inferred for the mass-loss rate-period relation, since at a given period mass-loss rates for LMC stars are in agreement with those observed in Galactic stars (see also Groenewegen et al. 2007). Despite a large spread at shorter periods, data suggest that the mass-loss rate increases strongly with period greater than $\log P \sim 2.6$. A less steep dependence can be argue at lower periods (see also Straniero et al. 2006), even if data (Galactic stars mostly) are more spread, as they suffer of the uncertainty on the distance, which appears in the expression used to derive mass-loss rate (see e.g. Whitelock et al. 2006).

From Figure 1 it appears that in the case of *model A* (panel *(a)*) the evolutionary lines nicely reproduce the observed trend. As a matter of fact, the bulk of stars are fairly reproduced by stars having masses approximatively in the range $\approx 1.4\div4.5 M_{\odot}$, and mass-loss rates reaching values as high as $\approx 8\times10^{-5} M_{\odot}$yr^{-1}. A few stars with higher mass-loss rates are O-rich stars belonging to the LMC field population (small open circles). Note that here we plot models with a single metallicity, while data refer to galaxy populations, consisting of a mixture of stars with different age, metallicity and mass. There are no studies that conclusively show that the mass-loss rate explicitly depends on metallicity (Zijlstra et al. 1996), however metallicity may have effect on grain growth, the number density and size of grains, thus altering the mass-loss rates from the stars. Finally, mass-loss rates may strongly depend on stellar pulsation. Stars of high metallicity, e.g. $Z = 0.02$, and mass are able to reach lower effective temperatures and higher mass-loss rates. In our models the central star typically has T_{eff} in the range $\sim 2500-3800$ K, in fair agreement with estimations found by Groenewegen et al. (2007) and van Loon et al. (2005) for MCs field populations, even thought the latter sample includes cooler stars. If $\eta^B = 1$ (*model B*) the mass-loss process is very efficient in stripping away the stellar envelope, and the evolution results steep and rapid. The formulation of van Loon et al. (2005) applied to our TP-AGB modeling produces a rapid increase of the mass-loss rate since the beginning of the phase (Figure 1, *model C*). The relation from van Loon (2007) produces a less steep behavior and longer periods at a given mass-loss rate (Figure 1, *model D*). However, we recall this formulation critically depends on A_V. In the rest of the paper, unless explicitly stated otherwise, we present results of models A and C, even though computations and comparison for models B and D have also been performed.

As conclusive remark, we notice that changing the mass-loss rate prescription may also affect the TP-AGB star structure, so that here we have performed a qualitative comparison between results of our synthetic modeling of TP-AGB stars and observations. The detailed treatment of the evolution of stars along the complex TP-AGB phase requires accurate TP-AGB evolution stellar models, for instance the modeling of the two stages (O- and C-rich phases) as a function of stellar mass and metallicity, by taking into account the internal structure evolution, stellar pulsation, mass-loss mechanism, and dust and grain formation (see e.g., Izzard et al. 2004; Marigo & Girardi 2007; Cristallo et al. 2009). Nevertheless, the agreement between the data and the general picture that we have presented is already very encouraging to investigate how these scenarios affect SBF predictions, as we do in the following sections.

2.3. *Integrated magnitudes*

To compute the cluster total fluxes we assume that the integrated luminosity is dominated by light emitted by their stellar component. On this basis, the total fluxes mainly depend on two quantities: *1)* the flux f_i emitted by the i-th star of mass M, age t, luminosity L, effective temperature T_{eff}, and chemical composition (Y, Z):

$$f_i[L(M,t,Y,Z), T_{eff}(M,t,Y,Z), Y, Z] \tag{6}$$

and *2)* the number of stars of mass M in a population counting N stars, $\Phi(M,N)$. f_i is defined by the stellar evolution library and the temperature-color transformation tables, while $\Phi(M,N)$ is strictly related to the

IMF. The Monte Carlo procedure we adopted is essential to simulate poorly populated stellar systems, like those we study in the following. It ensures that fast, undersampled evolutionary phases, are correctly treated from a stochastic point of view. The above quantities are combined to calculate the total integrated flux F in a given photometric band:

$$F[N,t,Y,Z] = \sum_{i=1}^{N} f_i. \tag{7}$$

To account for stochastic effects, we computed a large number (N_{sim}) of independent simulations for each set of population parameters (age, chemical composition, cluster mass, etc.). So that, we obtained statistical distributions of magnitudes (colors), produced by stochastic variations in the number and properties of bright and rare stars. For the purposes of this paper, $N_{sim} = 200$ is appropriate to reproduce the observed clusters (see also Figure 2 in Raimondo et al. 2005a).

The conversion from theoretical quantities to magnitudes and colors is based on the BaSeL library (Westera et al. 2002, and reference therein), with the exception of C- and O-rich stars, whose colors are derived from spectra of Lançon & Mouhcine (2002). The homogenized photometric system of Bessell & Brett (1988) is adopted, so that in the following magnitudes and colors involving the K filter are transformed into K_s filter according to Carpenter (2001). This assumption is adequate as extensively explained in Pessev et al. (2006).

2.4. *Surface Brightness fluctuations*

If the type and flux of stars that comprise the stellar population luminosity function are known, the SBF magnitude is defined as (Tonry & Schneider 1988):

$$\overline{M} = -2.5 \log \left[\frac{\sum_{i=1}^{N} f_i^2}{\sum_{i=1}^{N} f_i}\right] \tag{8}$$

where $\overline{M}$ relies upon the *Poissonian statistics*. This is the case of our synthetic stellar population models, in which the flux of each star is known. In the case of a large number of independent simulations, as adopted here, the average SBF magnitude can be defined as

$$\overline{M} = \frac{\sum_{j=1}^{N_{sim}} \overline{M}_j}{N_{sim}}, \tag{9}$$

and the statistical uncertainty is derived as the standard deviation of the $\overline{M}_j$ distribution ($j = 1, N_{sim}$).

3. CLUSTER SAMPLE AND DATA

The NIR photometry of 19 clusters in the LMC is from Ferraro et al. (2004) and Mucciarelli et al. (2006), obtained with the SOFI imager/spectrometer mounted on the ESO 3.5m NTT. Each cluster typically contains 1000-1200 objects, with the exception of a subsample of poorly populated clusters (such as NGC 2190, NGC 2209, NGC 2249, NGC 1651, NGC 2162, and NGC 2173) and an handful of rich clusters (such as NGC 1783, and NGC 1978) with more than 1900 stars.

The clusters are listed in Table 1 together with some properties. The age estimations from Mucciarelli et al. (2006) have been derived through the s-parameter calibration of Girardi et al. (1995), based on stellar models computed with a certain amount of convective overshoot. $[Fe/H]$ determinations from either spectroscopic or photometric data are also reported. The last three columns list the number of C-stars identified by various authors and the s-parameter from Elson & Fall (1985). The membership of C-rich giant stars is not well established in some cases. For instance, a giant star in NGC 2136/37 is identify as a C-star with $K \simeq 10.7$ mag and $J-K = 1.53$ mag since the work by Aaronson & Mould (1985), even its membership is not confirmed (Frogel et al. 1990).

We fixed the total V-magnitude of each cluster to be equal to the value published by Goudfrooij et al. (2006), who measured integrated-light photometry in Johnson-Cousins V, R and I for a sample of 28 star clusters in the MCs. From their Table A1 we selected measurements at an aperture radius corresponding to $1'.5$, the same area used to the CMD analysis (see below). For clusters not included in the sample of Goudfrooij et al. (2006), we consider measurements by van den Bergh (1981), bearing in mind that they generally refer to a smaller aperture size ($\sim$ 50-60$''$). After a rescaling, the formal difference between the two sets of measures is negligible, being of the order of $(V_G - V_V) = -0.03$ mag (Goudfrooij et al. 2006).

The distance modulus of LMC is settled to be $(m-M)_0 = 18.40 \pm 0.10$ mag, on the basis of recent estimations (e.g. Grocholski et al. 2007; Testa et al. 2007; Walker et al. 2001). It is worth mentioning that a variation of the LMC distance within the above uncertainty, e.g. the adoption of the usual distance value $(m-M)_0 = 18.50$ mag, does not affect the results presented below. Similar consideration can be done for the Galactic extinction law, here we use $R_V = 3.4$ (Gordon et al. 2003). The conversion of A_V to extinction coefficients in other photometric bands was done using formulae in Cardelli et al. (1989).

4. DATA/MODELS COMPARISON

The theoretical framework described in § 2 was adopted to derive fully consistent synthetic CMDs and integrated quantities. The comparison with *resolved* features of well studied star clusters (§ 3) provides the opportunity to calibrate NIR models in detail, by fitting the observed CMDs, star counts and luminosities, and at the same time integrated and SBF magnitudes. We take advantage of this joint analysis to infer indication on the efficiency of SBFs to estimate ages and metallicities of unresolved intermediate-age systems and to constrain the number and photometric properties of bright red giant stars.

4.1. *CMD, luminosity function and stellar counts*

The procedure to fit models to data can be summarized as follows. First, a series of synthetic CMDs were computed to estimate the age and chemical composition by fitting the observed CMD, and the cumulative luminosity function (CLF) of each cluster. The age step is 10% of the expected age, while the metallicity is given by the available grid of stellar evolution models, i.e. no-interpolation was done. Each synthetic CMD includes a fraction of detached binaries whose mass ratio was distributed homogeneously between 0.7 and 1, as found in several LMC clusters (e.g. NGC 1818: Elson et al. 1998; NGC 1866: Brocato et al. 2003; Barmina et al. 2002; NGC 2173: Bertelli et al. 2003). The fraction of binaries is a free parameter ranging from 10% up to 70% of the total. Age and metallicity evaluations are given by simultaneously fitting the distribution (CLF) and photometric properties (CMD) of stars in the cluster. Note that the computed cluster's V-magnitude (M_V^{tot}) is equal to the observed value. For the handful of clusters whose M_V^{tot} comes from the compilation of van den Bergh (1981), the systematic difference of the aperture-size was taken into account. Once the best-fitting parameters (age, metallicity, and fraction of binaries) were established, we computed a series of 200 synthetic CMDs in order to take into account stochastic effects (see § 2.3 and § 2.4). It is relevant to emphasize that random extractions of stellar masses are fully independent, even though the same set of input parameters is assumed. Moreover, when simulating the CMD we did not draw the same number of stars as observed, instead the number of stars placed in different regions of the synthetic CMD turns out from computations when the total magnitude is assumed to be equal to the observed one.

Figure 2 shows observed (left) and synthetic (right) $[K_s, J-K_s]$-CMD of each cluster. The synthetic CMD plotted is one of the 200 simulations computed in the framework of *model A*. C-type AGB stars are identified as stars, while M-type stars as asterisks. The vertical dotted lines indicate the rough separation between C-rich (redder) and O-rich (bluer) stars on the base of their $J-K_s$ color: $(J-K_s) \approx 1.4$ mag at $Z \geq 0.008$ and $(J-K_s) \approx 1.3$ mag at $Z = 0.004$, as empirically determined by Cioni et al. (2001, 2003) in the LMC and SMC and confirmed by the cross-correlation with spectroscopic surveys for example in SMC by Raimondo et al. (2005b). The clusters are arranged for increasing age, from 50 Myr to 5 Gyr. Metallicity ranges from $Z = 0.02$ down to $Z = 0.004$. The reddening value (E_{B-V}) labeled in each panel is the mean value of the measures available in the literature.

As pointed out by Mucciarelli et al. (2006) and Ferraro et al. (2004) a significant contribution of LMC field stars is present in all clusters (see their figures 1-4, and figures 2-4, respectively). However, in young clusters a blue sequence is clearly visible at $-0.3 \lesssim (J-K_s) \lesssim 0.3$ and $K_s \gtrsim 15.5$, corresponding to the brightest end of the cluster MS. At $K_s \sim 14$ mag the region occupied by He-burning stars is also recognized. So that, it is possible to confidently identify cluster's stars as those placed at the left of the solid lines reported in Figure 2 (first six plots), notwithstanding a residual uncertainty remains to establish the membership of stars with $K < 12-13$ mag (likely AGB stars). In the older clusters the observational limit ($K_s \approx 18.5$) does not permit to detect the TO point and for ages greater than ≈ 400 Myr it is not possible to easily identify field stars, since they overlap the cluster population. For all these reasons, to minimize the field contamination and to better estimate the cluster age and metallicity, the fit-procedure was applied to stars as far as $r = 1.5'$ off from the cluster center (large circles in the left panels of Figure 2), as suggested by Ferraro et al. (2004). In addition, we used the photometry of the control field a few arcmin away from each cluster to subtract the contribution of field stars to the observed CLF, after to have normalized and rescaled the data to the selected cluster's area. The resulting CLFs are used in the fit-procedure.

Figure 3 compares observed and synthetic CLFs. Synthetic CLFs well reproduce the observed counterparts, especially at $K_s \lesssim 17-17.5$ mag. This is a reliable limit free by crowding effects and completeness (Mucciarelli et al. 2006). For two clusters (NGC 1806 and NGC 1783) the agreement is limited to the brightest part of the CLF ($K_s \lesssim 14-15$ mag). Recent optical observations have suggested the presence of two stellar populations in the area of these two clusters, with an age difference of ≈ 300 Myr (Mackey et al. 2008). The NIR data used here do not permit to reach the TO point, however our best age estimation for NGC 1783 is about 1.2 Gyr, in fair agreement with the value recently suggested by Mucciarelli et al. (2007, $t \sim 1.4$ Gyr) and slightly younger than the interval suggested by Mackey et al. (2008, 1.6-2.2 Gyr), both derived from isochrones which include some overshooting. Other few clusters are recognized to be complex systems, for instance NGC 2136 and NGC 1987. The former is a component of a potential triple cluster system (Hilker et al. 1995). The latter is a very poorly-populated cluster lying in a highly field-contaminated region (Corsi et al. 1994; Ferraro et al. 2004), an occurrence that appears to be confirmed in Figure 3. Corsi and co-workers in their optical CMD discriminated three different populations: a very old field population, a young population producing a blue plume extending the bright MS, and the cluster population. Moreover, Frogel et al. (1990) identified two C-stars in the cluster area, whose membership, however, is determined uncertain for one of the two.

As our models *A-B-C-D* differ only for the treatment of the TP-AGB phase, there is a good agreement between observed and synthetic CMDs till the early-AGB either for *model A* or models *B*, *C* and *D*. Thus similar ages and metallicities are predicted from all the models. In contrast, the four models produced a different number of stars in the subsequent TP-AGB phase (see below).

Table 2 summarizes the age and metallicity, the mean M_V and M_{K_s} absolute magnitudes, and $J-K_s$ and $H-K_s$ colors (*models A*) for each cluster. As we used the available metallicity grid without making any interpolation, one can consider as metallicity uncertainty the difference between the best-fit value and the nearest two values in the grid.

From the age estimations in Table 2 and s values from Table 1 we obtain the following age-s parameter calibration (Figure 4*a*):

$$\log t = (5.37 \pm 0.12) + (0.099 \pm 0.003) \times s \tag{10}$$

Our calibration based on canonical stellar evolutionary tracks is compared to that of Girardi et al. (1995) and ages from the literature in Figure 4*b*. The use of both CMD and CLF has permitted to derive age estimations in agreement with those from the literature, however a future extension to the TO region will help in better define the age of some clusters, especially those for which recent deep optical-data have revealed the presence of multiple populations (e.g. NGC 1806 and NGC 1783, Mackey et al. 2008). Differences between the two calibrations are mostly due to the efficiency of overshooting in stellar convective H cores (Barmina et al. 2002; Brocato et al. 2003, and references therein).

We compare now the expected number of C-rich AGB stars derived from models *A*-*B*-*C*-*D* to the observed one. In Figure 5 the number of C-rich AGB stars normalized to the total visual light is plotted as a function of the TO mass (M_{TO}, Figure 5*a*) and the *s*-parameter (Figure 5*b*). The error budget of data accounts for the uncertainty of integrated visual light and the membership of C-stars, while theoretical uncertainty is estimated taking into account statistical fluctuations in the number of TP-AGB stars and the uncertainty of integrated visual light. As shown in Table 1, the number and luminosity of bright AGB stars may suffer a large statistical fluctuation in clusters of similar age. This is due to the small number statistics, as each cluster contains at most a few TP-AGB stars. This is visible in Figure 5*a* at $M_{TO} \sim 1.8-2.2$ M$_\odot$, where a few clusters having nearly the same age posses a different number of TP-AGB stars. Around these values there is a maximum in the frequency of the TP-AGB stars (see also Marigo & Girardi 2007). The qualitative analysis of Figure 5 also shows that the predicted trend is similar in all models, even thought the observed maximum is nicely reproduced by *model A*, and to a lesser extent *model D* and *C*. We find that in the mass range $1.7 \lesssim$ M/M$_\odot$ $\lesssim 2.5$ and for metallicity $Z = 0.008$ the TP-AGB lifetime is of the order of $\sim$ 2-3 Myr and reduces both at lower and higher masses. This result is in agreement with the analysis recently performed by Marigo & Girardi (2007).

4.2. *Integrated NIR colors*

TP-AGB stars affect NIR-bands integrated luminosity and its uncertainty in low-metallicity intermediate-age massive clusters (see e.g. Girardi & Bertelli 1998; Maraston 1998; Mouhcine & Lançon 2002; Maraston 2005). In particular, NIR colors may be dominated by a handful of red giant stars (Santos & Frogel 1997; Brocato et al. 1999a; Cerviño & Valls-Gabaud 2003). At the typical age of Galactic globular clusters (GGC), the presence of C-rich stars becomes more uncertain, as in GGC AGB stars are all observed to be O-rich, so that carbon does not appear to have been dredged up into the envelop during thermal pulses (Habing & Olofsson 2003). It is worth noting that the assumption on mass loss is expected to have a marginal effect on integrated magnitudes and colors of very faint populations, where bright TP-AGB stars are statistically less frequent, or even absent (Santos & Frogel 1997; Fagiolini et al. 2007).

The differences between observed and predicted magnitudes (colors) of each cluster are plotted for models *A* and *C* in Figure 6 and Figure 7, respectively. Theoretical values are calculated as the average over 200 simulations (see § 2.3), and error-bars are related to the standard deviation (1σ). Simulated values of M_V^{tot} are compared to measurements of Goudfrooij et al. (2006) or van den Bergh (1981) (left higher panel), while predicted values of M_{K_s} and colors ($J - K_s$ and $H - K_s$) are compared to data from Pessev et al. (2006, top), Mucciarelli et al. (2006, middle), and Persson et al. (1983, bottom). Observations are decontaminated for the field contribution, and dereddened by using the mean E_{B-V} values labelled in Figure 2.

Figure 6 shows that the agreement is nice for all the clusters in the case of Pessev et al. (2006) and Mucciarelli et al. (2006), while a discrepancy can be seen with Persson et al. (1983). As pointed out by Pessev et al. (2006), a major discrepancy between their color measurements with those of Persson et al. (1983) are caused by centering problems and to the presence of several relatively bright stars in the background field. In the figure it is clearly shown that colors of low-luminosity clusters have a large dispersion (see also Santos & Frogel 1997; Brocato et al. 1999a; Fagiolini et al. 2007). This is the case of the faint cluster NGC 2209, for which Pessev et al. (2006) recognize the major difference with Persson et al. (1983). For this cluster we estimated an age $\log t = 8.95 \pm 0.10$, in agreement with our previous value from optical-HST data (Raimondo et al. 2005a). The cluster contains two C-stars, identified by Walker (1971) and confirmed by Frogel et al. (1990), dominating NIR fluxes. No M-giants are possessed by the cluster.

Inspection in Figure 7 shows that predicted K_s magnitudes still agree with observations within the errorbars, especially in the case of data from Pessev et al. (2006) and Mucciarelli et al. (2006). With a few exceptions, differences between observed and predicted colors are contained in the region marked by the dotted lines, illustrating all the color values covered by simulations. Thus, synthetic colors are still able to reproduce the data in the case of models *C*, even if the agreement worsens at redder colors (i.e. $J - K_s \gtrsim 1$ mag and $H - K_s \gtrsim 0.3$ mag), as a consequence of the smaller number of TP-AGB stars predicted by *model C* compared to *model A*. Nearly the same results can be inferred from the analysis of colors from *model D*, and slightly worsen for *model B* (see Figure 8), where for sake of brevity only differences between observed and predicted K_s-magnitudes and $(J - K_s)$ colors are reported.

In conclusion, observed NIR magnitudes and colors of LMC clusters are reproduced by *model A*, and to a lesser extent by *model C*, *D*, and *B* (the worst case), within errorbars or at least within the color distributions obtained from all the simulations (200) computed for each cluster. Therefore, even though NIR integrated magnitudes and colors are sensitive to TP-AGB stars, they do not appear to be efficient enough to discriminate among physical assumptions which affect the number of bright TP-AGB stars in clusters, at least for the degree of accuracy of models proposed here (§ 2.2).

4.3. *Surface Brightness Fluctuations*

In this section we present observed SBF magnitudes of individual clusters and compare them with theoretical predictions. In the case of star clusters the SBF measurements are obtained from the second moment of the stellar luminosity function directly derived from resolved-star photometry (Ajhar & Tonry 1994; González et al. 2004; Raimondo et al. 2005a). Let us recall that this procedure measures the *same* physical quantity obtained for galaxies, and derived from the pixel-to-pixel brightness variation in the galaxy image. Studying SBFs of LMC star clusters is then a relevant step to understand the SBF signal from unresolved galaxies where light is (totally or partially) emitted by the underlying mixture of old and intermediate-age populations.

SBF magnitudes of clusters were estimated as follows. We coupled individual stellar photometry and total fluxes of the clusters both provided by Mucciarelli et al. (2006). The denominator is the cluster total flux, free from field contamination and reddening. The depth of the stellar photometry used here, contributing to the numerator, is adequate for our purposes. In fact, as discussed by Ajhar & Tonry (1994), in the optical and at least for halo GGGs, the second moment of the luminosity (numerator), converges quickly, with 99% of the sum being obtained with the three brightest magnitudes of cluster stars. This is even more evident in NIR bands (González et al. 2004), where the total light is dominated typically by RGB and AGB stars in populations older than a few hundreds of Myr. For sake of consistency with the analysis in § 4.1, we consider only stars within $1.5'$. As already noted, even in this restricted area, field stars are distinguishable from cluster stars only in the youngest clusters, since in the remaining ones giant stars belonging to the cluster and to the field occupy the same regions of the CMD (see Figure 2). Consequently, the contribution of field stars to the numerator can be easily subtracted for the first six clusters. In older clusters we used the control-field frames, assuming that the field stellar population present in the adjacent field is identical to that populating the cluster's area. The procedure was applied to each cluster of the sample and results are reported in Table 3. The errorbars also include the effect due to the uncertainty on the membership of bright stars.

We calculated theoretical SBFs from the exact simulations used to reproduce the CMDs, CLFs, integrated magnitudes and colors. In practice, for a given cluster SBF amplitudes were derived applying Eq. 8 and 9. In Figures 9 and 10 we plot differences between observed and predicted SBFs (*model A* and *model C*, respectively) as a function of the observed M_J and M_{K_s} magnitudes. Differently from colors, that are reproduced by both assumptions (even if with different precision), the SBF data/models comparison shows a clear different behavior. SBFs from *model A* provide a good agreement with data in the entire range of M_J and M_{K_s}, being differences mostly lower or of the order of ~ 0.5 mag. There are only three outlayers, namely NGC 2134 and, at less extent, NGC 1783 and NGC 1806, in which a high field contamination was recognized (Figure 3). On the other hand, *model C* foresees SBFs fainter than the observed ones, in particular this model underestimates the number of bright stars in the magnitude intervals $-8 \lesssim M_J \lesssim -9$ and $-9 \lesssim M_K \lesssim -9.8$ (Figure 10).

To better interpret these results, Figure 11 shows the relationship between SBF differences and s-parameter (age). Again, in the case of *model A* the agreement is good for all the s-parameter values considered here. On the other hand, it is clear that clusters with $s > 30$ (ages greater than about 200 Myr), i.e. the age at which the number of TP-AGB stars becomes statistically relevant, suffer large discrepancy in the case of *model C*. Although the sample does not contain very old clusters, our guess is that for ages older than ∼5 Gyr the effect should decrease, as already shown in Raimondo et al. (2005a). Note that results from *model B* and *D* show a behavior similar to *model C*. Thus, changing the number of TP-AGB stars mainly affect the SWB classes IV, V and VI (see also Figure 5). We recall the four models (*A*-*D*) differ only for the treatment of the mass-loss process of TP-AGB stars. On this basis, we suggest that *model A* is more appropriate to reproduce the SBF measurements of LMC star clusters in the range $30 < s < 45$, where TP-AGB stars are expected to have a large impact on the cluster observational properties. It is worth noting that this conclusion is not unique and should be verified when different assumptions are used in stellar population models (e.g. IMF, stellar evolutionary tracks, color-temperature relations, TP-AGB synthetic prescriptions, etc.). Within this limitation, we suggest that SBFs can contribute to disentangle the observable properties of TP-AGB stars in unresolved galaxies containing a large number of such stars.

Before concluding this section, we compare present SBF measurements to those by González et al. (2004). They derived NIR-SBFs of star clusters in the MCs as grouped (to obtain a sort of super-clusters) according to SWB classes (Searle et al. 1980). This procedure allows the authors to reduce the problem of small number statistics, and to compare LMC cluster data to SBF predictions computed for systems with a large number of stars, i.e. galaxies (see Raimondo et al. 2005a, for details). We grouped the present clusters using the same definition of SWB classes. Our sample does not cover the Pre, SWB-I and VII classes. Moreover, the SWB-II class contains only one cluster (NGC2164), thus it is not significative. Table 4 summarizes the cluster grouping and the resulting SBF data. Figure 12 compares SBF data of super-clusters from both sets of measures. Despite the smaller number of clusters considered in the present work, the agreement between the two sets of measurements is quite good, even though there is a systematic age shift of SWB-III and SWB-V due to the different *s*-parameter/age relation. González et al. (2004) assigned ages and metallicities to the super-clusters from Frogel et al. (1990), with a few exceptions regarding SWB-I, SWB-II and Pre-SWB super-cluster. The open stars in Figure 12 result from grouping the corresponding synthetic CMDs, i.e. we applied exactly the same procedure used for observations. The proper SWB class is assigned according to the present age estimations of each cluster, then a mean is considered. We note a slight discrepancy (<0.5 mag) for SWB-VI in the *J*-band and for SWB-V in the K_s-band. We recall that for these two classes the overlapping between cluster and field population is more severe. As a conclusion, we note that the data/models comparison for super-clusters stands again for a consistency of the present procedure and SPS models.

5. SUMMARY AND CONCLUSIONS

In this paper we carried out a joint analysis of *resolved* and *unresolved* properties of a sample of LMC clusters, in order to consistently derive the evolutionary status of stars in the clusters, by using different stellar population synthesis tools based on an unique theoretical framework. The final aim was understanding the potential of the SBF technique as tracer of stellar populations, and exploring the use of such a technique to constrain more tightly stellar population models, those of intermediate age in particular.

To reach this goal, we studied the CMD, CLF, integrated magnitudes and colors, and SBFs of 19 LMC star clusters, covering an age range from a few Myr up to several Gyr. We used accurate NIR (J and K_s bands) photometric data of cluster's resolved stars (Ferraro et al. 2004; Mucciarelli et al. 2006), and NIR colors from up-to-date compilations by Goudfrooij et al. (2006), Pessev et al. (2006) and Mucciarelli et al. (2006). By coupling resolved star photometry with total fluxes, we derived new measurements of NIR-SBFs for each individual cluster, paying attention to field star contamination which may highly affect stellar counts in the upper part of the luminosity function. This allows us to obtain a set of homogeneous and high-quality SBF data of pure intermediate-age stellar populations. This is a necessary step toward having a larger sample of star clusters with accurate measurements of SBFs.

We used the multi-purpose synthesis code *SPoT*, based on a unique and consistent theoretical framework, to predict all the quantities quoted above. Great attention was payed to take into account stochastic effects. This is a crucial point, as broad-band colors and, in general, spectro-photometric features of clusters may suffer from large *intrinsic* fluctuations caused by the discrete nature of the number of stars (see e.g. Barbaro & Bertelli 1977; Chiosi et al. 1988; Santos & Frogel 1997; Brocato et al. 1999a; Raimondo et al. 2005a). Therefore, including stochastic effects is an important step to derive reliable age and metallicity estimations from cluster broad-band colors (e.g. Fagiolini et al. 2007).

We also presented new synthesis models (*A-D* in Sect. 2.2), computed under the same prescriptions for all the evolutionary phases except for the mass-loss rates of TP-AGB stars. Model results were compared to data through the fitting of observed CMD, CLF, and integrated colors of each cluster. The agreement obtained in reproducing both *resolved* and *unresolved* observational quantities suggests a high degree of reliability of the adopted theoretical framework. The cluster ages and metallicities derived by best-fit models are also in agreement (within the uncertainties) with previous determinations from other indicators. The age estimates were used to derive a new calibration of the s-parameter/age relationship for intermediate-age stellar clusters, i.e. s values within the range 20-45.

Following the same line presented in Raimondo et al. (2005a), we showed that NIR-SBFs are extremely sensitive to the number and properties of AGB (especially TP-AGB) stars. Changing the mass-loss rate prescription affects TP-AGB properties, including the duration of the entire phase and thus SBF predictions change sizably. On the basis of the theoretical framework adopted (WG98 and W90) to describe the TP-AGB evolution, we found that although all the models are able to reproduce observed CMDs, CLFs and integrated magnitudes and colors, even though with different precision, not all the models reproduce the SBF measurements of LMC clusters. In particular, only *model A* provides a good fit of NIR-SBF in the age range corresponding to $30 < s < 45$, where TP-AGB stars are expected to be more numerous. Thus, we argue that the global theoretical scenario adopted in *model A* appears to be able to reproduce all the observational properties of the LMC star clusters investigated in this work. It is worth noticing that the theoretical prescriptions used for modeling stellar clusters may affect our results on TP-AGB synthetic evolution, for instance the luminosity and effective temperature at the first thermal pulse. In this sense, an effort to study the physics of AGB structure experiencing thermal pulses is urged to provide solid theoretical background for stellar population synthesis studies. In spite of this limit, we showed that NIR-SBFs are very sensitive to the properties of TP-AGB stars, then they can be useful to investigate the global nature of such stars in clusters and galaxies, where they are numerous and statistical effects are less important. Using the large and homogeneous sample of clusters presented here, we have shown that SBF amplitudes may be linked to stellar evolution properties, and, in turn, they can be used as an intriguing and complementary diagnostic to test the ingredients of SPS models, and evolution properties of bright giant stars.

As conclusive discussion, we notice that the metallicity dependence of the C-rich phase lifetime was accounted for using the relationship between the number ratio of C- to M-stars and the metallicity observed for the Local Group galaxies (Groenewegen 2007). However, the number ratio of C-rich/O-rich stars should be a complex function of the properties of individual AGB stars, i.e. the durations of the entire phase and the subphases (O/C-rich, respectively), and the location of AGB stars in the CMD. Moreover, even though the use of a purely synthetic code to describe the TP-AGB phase is less accurate than the full stellar modeling, it is the only way to explore a large parameter space in computing SPS models. The uncertainties in assigning – as well as in predicting– stellar parameters of variable TP-AGB stars (e.g. effective temperature, opacity, luminosity), where effects such as convection, variability, mass loss, and dust formation become increasingly important (Freytag & Höfner 2008), still have a great impact in SPS models. Modern stellar evolutionary codes as well as hydrodynamical codes for stellar atmospheres are at present extensively used to model different aspects of stellar physics at work in stars beyond the core-helium burning phase, as the interior nucleosynthesis and envelope chemical enrichment and their dependence on stellar metallicity and mass, hence we expect to reduce the uncertainty of the predicted properties of AGB stars and then of intermediate-age stellar population models in the next future. Once again detailed analysis and accurate simulations of well-known stellar populations like LMC star clusters represent a fundamental step to improve our understanding of the nature of contributors to the integrated light from remote galaxies, as well as the potential of SBFs to disentangle the evolutionary status of unresolved populations.

We warmly thank Alessio Mucciarelli and Francesco Ferraro for providing us photometric data, and Adriano Pietrinferni and Santi Cassisi for updated stellar evolution models. It is a pleasure to thank Enzo Brocato and Michele Cantiello for useful discussions on the subject. This work received financial support by INAF-PRIN/06 (PI G.C.). We acknowledge the anonymous referee for comments and suggestions which greatly improved the paper.

REFERENCES

Aaronson, M., & Mould, J. 1985, ApJ, 288, 551
Ajhar, E. A., & Tonry, J. L. 1994, ApJ, 429, 557
Barbaro, C., & Bertelli, C. 1977, A&A, 54, 243
Barmina, R., Girardi, L., & Chiosi, C. 2002, A&A, 385, 847
Bertelli, G., Nasi, E., Girardi, L., Chiosi, C., Zoccali, M., & Gallart, C. 2003, AJ, 125, 770
Bessell, M. S., & Brett, J. M. 1988, PASP, 100, 1134
Blakeslee, J. P., Vazdekis, A., & Ajhar, E. A. 2001, MNRAS, 320, 193
Bloecker, T. 1995, A&A, 297, 727
Bowen, G. H. 1988, ApJ, 329, 299
Bressan, A., Chiosi, C., & Fagotto, F. 1994, ApJS, 94, 63
Brocato, E., Cassisi, S., & Castellani, V. 1998, MNRAS, 295, 711
Brocato, E., Castellani, V., Di Carlo, E., Raimondo, G., & Walker, A. R. 2003, AJ, 125, 3111
Brocato, E., Castellani, V., Poli, F. M., & Raimondo, G. 2000, A&AS, 146, 91
Brocato, E., Castellani, V., Raimondo, G., & Romaniello, M. 1999a, A&AS, 136, 65
Brocato, E., Castellani, V., Raimondo, G., & Walker, A. R. 1999b, ApJ, 527, 230
Bruzual, G., & Charlot, S. 2003, MNRAS, 344, 1000
Cantiello, M., Blakeslee, J., Raimondo, G., Brocato, E., & Capaccioli, M. 2007, ApJ, 668, 130
Cantiello, M., Blakeslee, J. P., Raimondo, G., Mei, S., Brocato, E., & Capaccioli, M. 2005, ApJ, 634, 239
Cantiello, M., Raimondo, G., Brocato, E., & Capaccioli, M. 2003, AJ, 125, 2783
Cardelli, J. A., Clayton, G. C., & Mathis, J. S. 1989, ApJ, 345, 245
Carpenter, J. M. 2001, AJ, 121, 2851
Cerviño, M., & Valls-Gabaud, D. 2003, MNRAS, 338, 481
Chabrier, G., & Mera, D. 1997, A&A, 328, 83
Chiosi, C., Bertelli, G., & Bressan, A. 1988, A&A, 196, 84
Cioni, M.-R. L. et al. 2003, A&A, 406, 51
Cioni, M.-R. L., Marquette, J.-B., Loup, C., Azzopardi, M., Habing, H. J., Lasserre, T., & Lesquoy, E. 2001, A&A, 377, 945
Corsi, C. E., Buonanno, R., Fusi Pecci, F., Ferraro, F. R., Testa, V., & Greggio, L. 1994, MNRAS, 271, 385
Cristallo, S., Straniero, O., Gallino, R., Lederer, M. T., Piersanti, L., & Domínguez, I. 2008, in American Institute of Physics Conference Series, Vol. 1001, Evolution and Nucleosynthesis in AGB Stars, ed. R. Guandalini, S. Palmerini, & M. Busso, 3–10
Cristallo, S., Straniero, O., Gallino, R., Piersanti, L., Domínguez, I., & Lederer, M. T. 2009, ApJ, 696, 797
Dirsch, B., Richtler, T., Gieren, W. P., & Hilker, M. 2000, A&A, 360, 133
Elson, R. A. W. 1991, ApJS, 76, 185
Elson, R. A. W., & Fall, S. M. 1985, ApJ, 299, 211
—. 1988, AJ, 96, 1383
Elson, R. A. W., Sigurdsson, S., Davies, M., Hurley, J., & Gilmore, G. 1998, MNRAS, 300, 857
Fagiolini, M., Raimondo, G., & Degl'Innocenti, S. 2007, A&A, 462, 107
Ferraro, F. R., Origlia, L., Testa, V., & Maraston, C. 2004, ApJ, 608, 772
Fox, M. W., & Wood, P. R. 1982, ApJ, 259, 198
Freytag, B., & Höfner, S. 2008, A&A, 483, 571
Frogel, J. A., Mould, J., & Blanco, V. M. 1990, ApJ, 352, 96
Geisler, D., Bica, E., Dottori, H., Claria, J. J., Piatti, A. E., & Santos, Jr., J. F. C. 1997, AJ, 114, 1920
Girardi, L., & Bertelli, G. 1998, MNRAS, 300, 533
Girardi, L., Chiosi, C., Bertelli, G., & Bressan, A. 1995, A&A, 298, 87
González, R. A., Liu, M. C., & Bruzual A., G. 2004, ApJ, 611, 270
Gordon, K. D., Clayton, G. C., Misselt, K. A., Landolt, A. U., & Wolff, M. J. 2003, ApJ, 594, 279
Goudfrooij, P., Gilmore, D., Kissler-Patig, M., & Maraston, C. 2006, MNRAS, 369, 697
Grocholski, A. J., Cole, A. A., Sarajedini, A., Geisler, D., & Smith, V. V. 2006, AJ, 132, 1630
Grocholski, A. J., Sarajedini, A., Olsen, K. A. G., Tiede, G. P., & Mancone, C. L. 2007, AJ, 134, 680
Groenewegen, M. A. T. 2007, in Astronomical Society of the Pacific Conference Series, Vol. 378, Why Galaxies Care About AGB Stars: Their Importance as Actors and Probes, ed. F. Kerschbaum, C. Charbonnel, & R. F. Wing, 433–+
Groenewegen, M. A. T., & de Jong, T. 1994, A&A, 288, 782
Groenewegen, M. A. T. et al. 2007, MNRAS, 376, 313
Habing, H. J., & Olofsson, H., eds. 2003, Asymptotic giant branch stars, ed. H. J. Habing & H. Olofsson
Heras, A. M., & Hony, S. 2005, A&A, 439, 171
Herwig, F. 2008, in IAU Symposium, Vol. 252, IAU Symposium, ed. L. Deng & K. L. Chan, 205–213
Hilker, M., Richtler, T., & Stein, D. 1995, A&A, 299, L37+
Hill, V., François, P., Spite, M., Primas, F., & Spite, F. 2000, A&A, 364, L19
Iben, Jr., I., & Renzini, A. 1983, ARA&A, 21, 271
Izzard, R. G., Tout, C. A., Karakas, A. I., & Pols, O. R. 2004, MNRAS, 350, 407
Jensen, J. B., Tonry, J. L., Barris, B. J., Thompson, R. I., Liu, M. C., Rieke, M. J., Ajhar, E. A., & Blakeslee, J. P. 2003, ApJ, 583, 712
Kitsikis, A., & Weiss, A. 2007, in Astronomical Society of the Pacific Conference Series, Vol. 378, Why Galaxies Care About AGB Stars: Their Importance as Actors and Probes, ed. F. Kerschbaum, C. Charbonnel, & R. F. Wing, 99–+
Kroupa, P. 2001, MNRAS, 322, 231
Lançon, A., & Mouhcine, M. 2002, A&A, 393, 167
Liu, M. C., Charlot, S., & Graham, J. R. 2000, ApJ, 543, 644
Liu, M. C., Graham, J. R., & Charlot, S. 2002, ApJ, 564, 216
Mackey, A. D., Broby Nielsen, P., Ferguson, A. M. N., & Richardson, J. C. 2008, ApJ, 681, L17
Mackey, A. D., & Gilmore, G. F. 2003, MNRAS, 338, 85
Maraston, C. 1998, MNRAS, 300, 872
—. 2005, MNRAS, 362, 799
Marigo, P. 1998, A&A, 340, 463
Marigo, P., & Girardi, L. 2007, A&A, 469, 239
Marigo, P., Girardi, L., & Bressan, A. 1999, A&A, 344, 123
Mouhcine, M., González, R. A., & Liu, M. C. 2005, MNRAS, 362, 1208
Mouhcine, M., & Lançon, A. 2002, A&A, 393, 149
Mucciarelli, A., Origlia, L., & Ferraro, F. R. 2007, AJ, 134, 1813
Mucciarelli, A., Origlia, L., Ferraro, F. R., Maraston, C., & Testa, V. 2006, ApJ, 646, 939
Olszewski, E. W., Schommer, R. A., Suntzeff, N. B., & Harris, H. C. 1991, AJ, 101, 515
Persson, S. E., Aaronson, M., Cohen, J. G., Frogel, J. A., & Matthews, K. 1983, ApJ, 266, 105
Pessev, P. M., Goudfrooij, P., Puzia, T. H., & Chandar, R. 2006, AJ, 132, 781
Pietrinferni, A., Cassisi, S., Salaris, M., & Castelli, F. 2004, ApJ, 612, 168
Raimondo, G., Brocato, E., Cantiello, M., & Capaccioli, M. 2005a, AJ, 130, 2625
Raimondo, G., Castellani, V., Cassisi, S., Brocato, E., & Piotto, G. 2002, ApJ, 569, 975
Raimondo, G., Cioni, M.-R. L., Rejkuba, M., & Silva, D. R. 2005b, A&A, 438, 521
Renzini, A. 2006, ARA&A, 44, 141
Renzini, A., & Voli, M. 1981, A&A, 94, 175
Sagar, R., & Pandey, A. K. 1989, A&AS, 79, 407
Santos, Jr., J. F. C., & Frogel, J. A. 1997, ApJ, 479, 764
Schöier, F. L., & Olofsson, H. 2001, A&A, 368, 969
Searle, L., Wilkinson, A., & Bagnuolo, W. G. 1980, ApJ, 239, 803
Straniero, O., Chieffi, A., Limongi, M., Busso, M., Gallino, R., & Arlandini, C. 1997, ApJ, 478, 332
Straniero, O., Domínguez, I., Cristallo, R., & Gallino, R. 2003, Publications of the Astronomical Society of Australia, 20, 389
Straniero, O., Gallino, R., & Cristallo, S. 2006, Nuclear Physics A, 777, 311
Testa, V. et al. 2007, A&A, 462, 599
Tonry, J., & Schneider, D. P. 1988, AJ, 96, 807
Tonry, J. L., Ajhar, E. A., & Luppino, G. A. 1990, AJ, 100, 1416
Tonry, J. L., Dressler, A., Blakeslee, J. P., Ajhar, E. A., Fletcher, A. B., Luppino, G. A., Metzger, M. R., & Moore, C. B. 2001, ApJ, 546, 681
van den Bergh, S. 1981, A&AS, 46, 79

van Loon, J. T. 2007, in Astronomical Society of the Pacific Conference Series, Vol. 378, Why Galaxies Care About AGB Stars: Their Importance as Actors and Probes, ed. F. Kerschbaum, C. Charbonnel, & R. F. Wing, 227–+
van Loon, J. T., Cioni, M.-R. L., Zijlstra, A. A., & Loup, C. 2005, A&A, 438, 273
Wachter, A., Schröder, K.-P., Winters, J. M., Arndt, T. U., & Sedlmayr, E. 2002, A&A, 384, 452
Wagenhuber, J., & Groenewegen, M. A. T. 1998, A&A, 340, 183
Walker, A. R., Raimondo, G., Di Carlo, E., Brocato, E., Castellani, V., & Hill, V. 2001, ApJ, 560, L139
Walker, M. F. 1971, ApJ, 167, 1
Westera, P., Lejeune, T., Buser, R., Cuisinier, F., & Bruzual, G. 2002, A&A, 381, 524
Westerlund, B. E., Azzopardi, M., Rebeirot, E., & Breysacher, J. 1991, A&AS, 91, 425
Whitelock, P. A., Feast, M. W., Marang, F., & Groenewegen, M. A. T. 2006, MNRAS, 369, 751
Whitelock, P. A., Feast, M. W., van Loon, J. T., & Zijlstra, A. A. 2003, MNRAS, 342, 86
Winters, J. M., Le Bertre, T., Jeong, K. S., Nyman, L.-Å., & Epchtein, N. 2003, A&A, 409, 715
Wood, P. R. 1990, in From Miras to Planetary Nebulae: Which Path for Stellar Evolution?, ed. M. O. Mennessier & A. Omont, 67–84
Worthey, G. 1993, ApJ, 409, 530
Zijlstra, A. A., Loup, C., Waters, L. B. F. M., Whitelock, P. A., van Loon, J. T., & Guglielmo, F. 1996, MNRAS, 279, 32

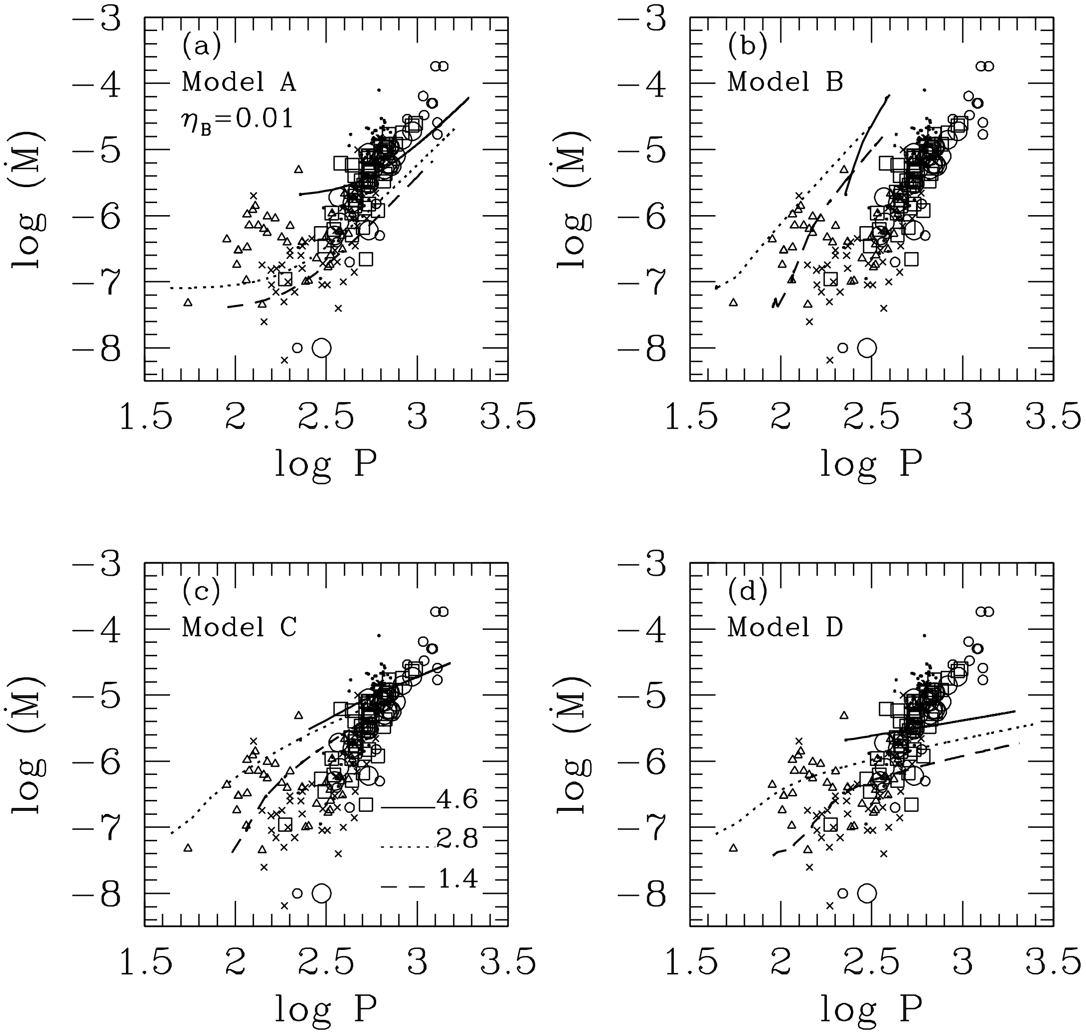

Fig. 1.— Observed periods and mass-loss rates of AGB stars from the literature: O-rich and C-rich stars in the LMC (Whitelock et al. 2003, small and big open circles, respectively); C-stars of LMC (Groenewegen et al. 2007, squares); Galactic C-rich stars from Whitelock et al. (2006, dots) and Schöier & Olofsson (2001, crosses); Galactic AGB stars (Winters et al. 2003, triangles). Data are compared to the theoretical sequences of three masses as labeled, metallicity $Z = 0.008$, and mass-loss formulations from: Bloecker (1995) with $\eta^B = 0.01$ ($M \geq 1.2\,\mathrm{M}_\odot$) and Wachter et al. (2002) ($M < 1.2\,\mathrm{M}_\odot$) in panel (*a*); Bloecker (1995) with $\eta^B = 1$ for all masses in panel (*b*); van Loon et al. (2005) and van Loon (2007) in panel (*c*) and (*d*), respectively.

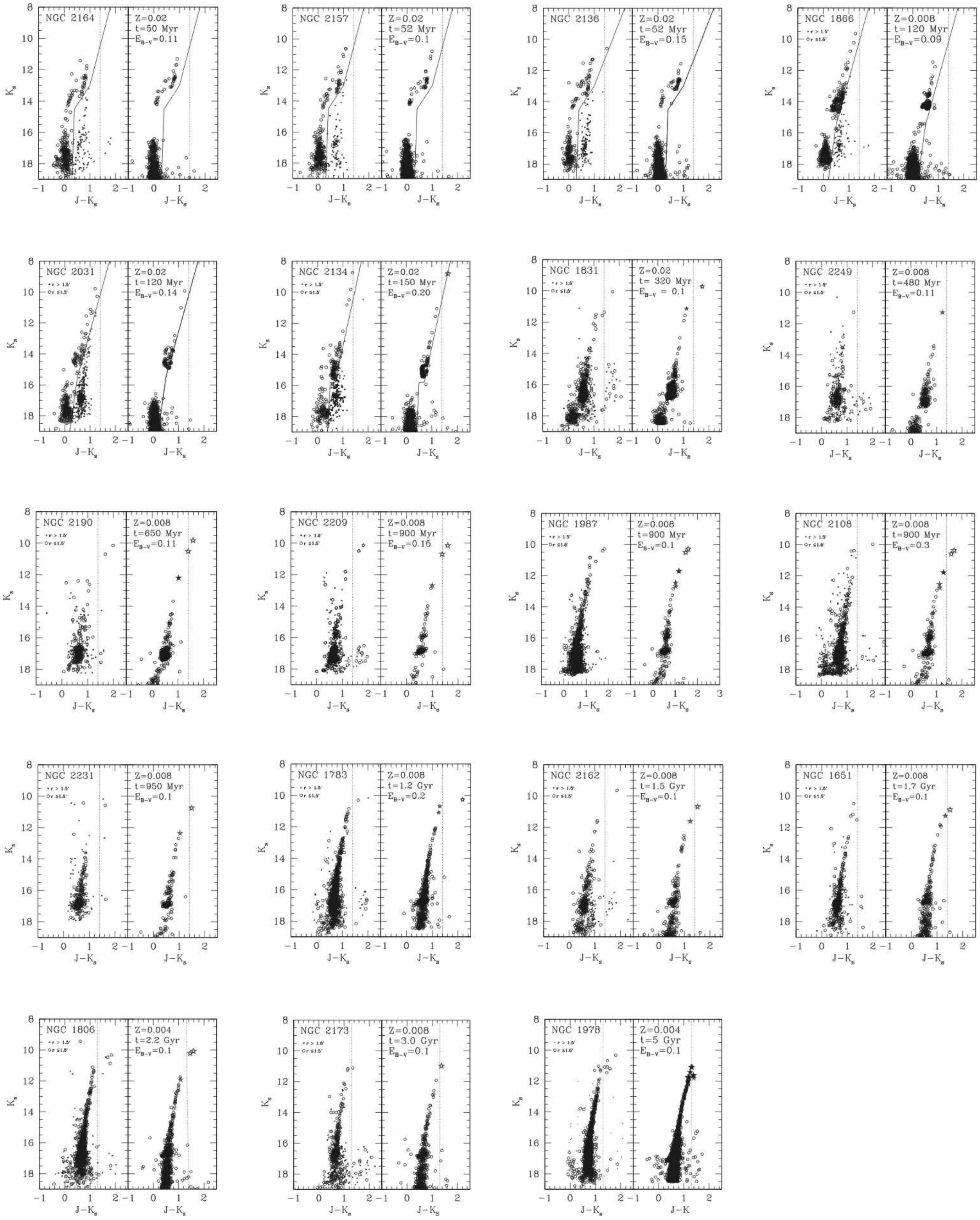

FIG. 2.— Left panels: Observed NIR-CMDs. Stars within 1′.5 are plotted as larger circles, while stars at $r > 1'.5$ as dots. We plot sources which were detected in both J and K_s bands and have no artifacts in these bands. In the first six clusters the CMD region at the left (right) of the solid line is likely dominated by the cluster (field) population. Right panels: One of the simulated CMDs (*model A*). The adopted metallicity (Z), age and E_{B-V} are labeled from top to bottom. Predicted C-rich and O-rich TP-AGB stars are indicated as stars and asterisks, respectively. The vertical dotted lines indicate the rough separation between O- and C-rich stars based on their $J - K_s$ color (see text).

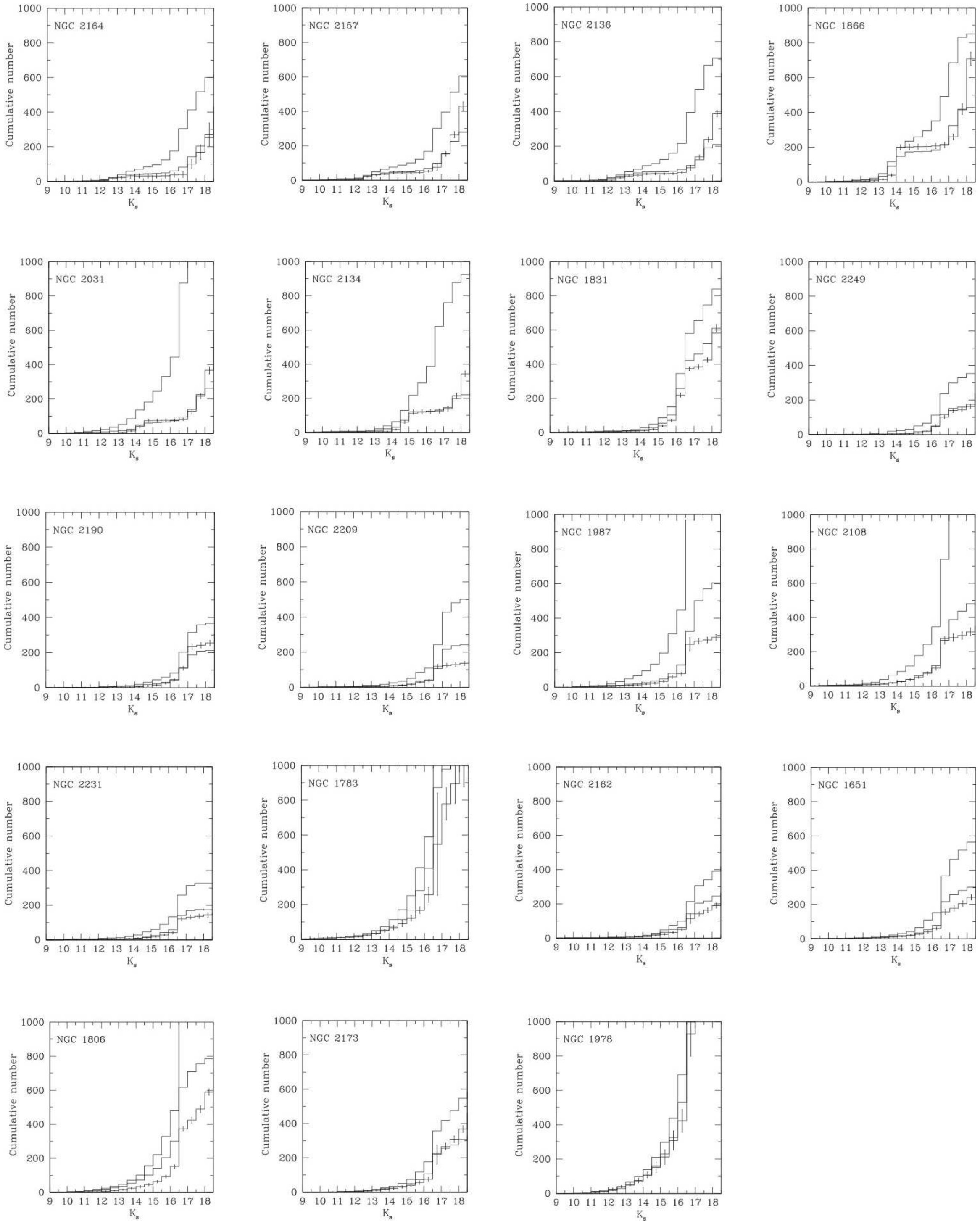

FIG. 3.— Cumulative K_s-LF (CLF) of each cluster: Dotted lines are CLFs from all observed stars, long-dashed lines are CLFs after the subtraction of field stars. Only the cluster's area within $1'.5$ is considered. Solid lines represent the mean synthetic CLF obtained from 200 simulations in the framework of *model A*. The estimated error is also plotted in each bin.

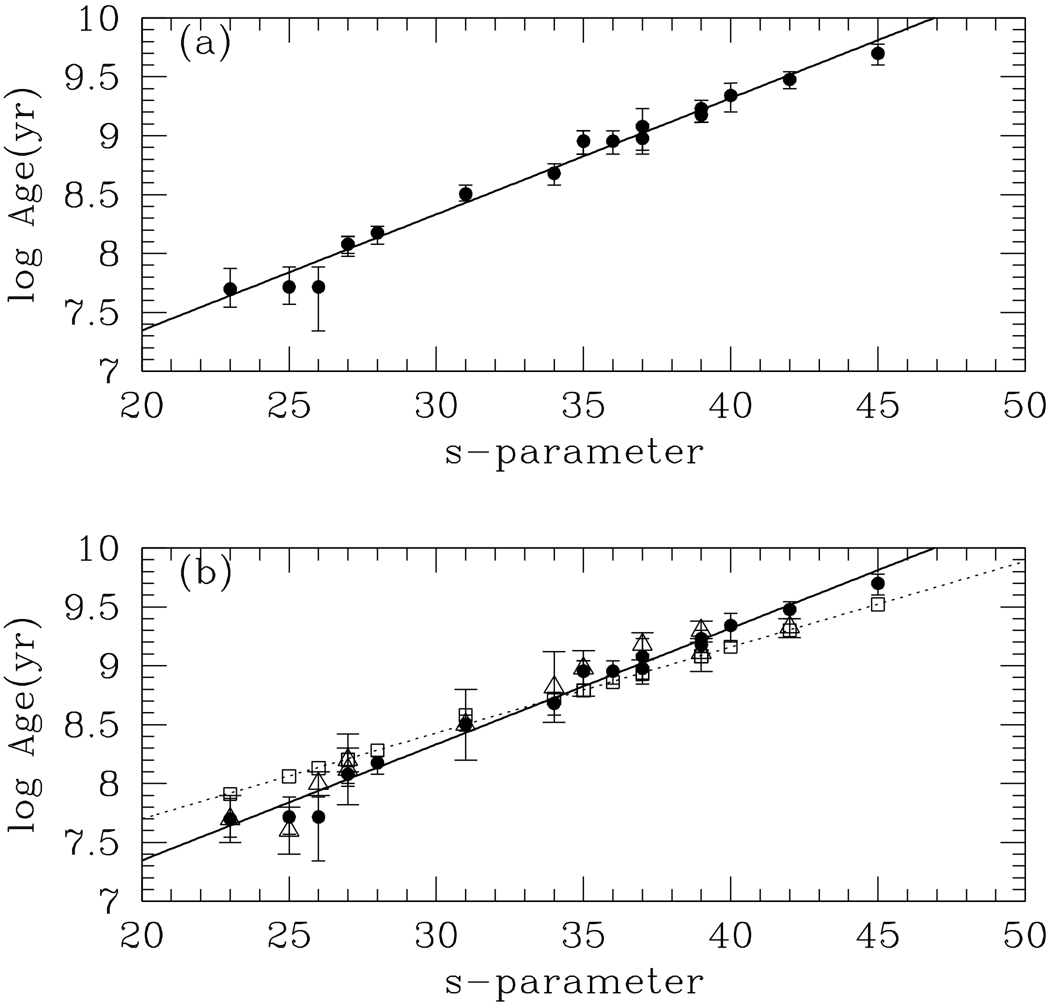

FIG. 4.— Panel (a): Age estimations (filled circles) and age-*s* calibration (solid line) from the present analysis. The *s* parameter comes from Elson & Fall (1985). Panel (b): The present age-*s* calibration (solid line) is compared to ages from (Mucciarelli et al. 2006, open squares, dotted line), and ages estimated from the CMD by various authors (see Col.2 in Table 1, open triangles).

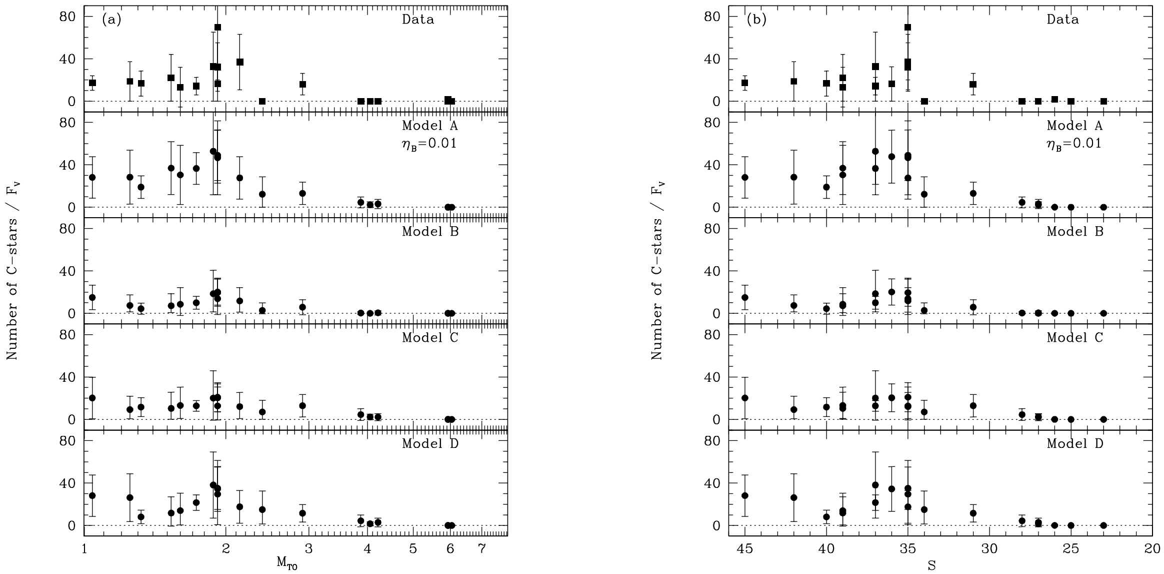

FIG. 5.— The number of C-rich stars normalized to the total V luminosity of the cluster is reported as a function of the TO mass (left) and s-parameter (right) for individual clusters. Squares represent data (upper panels), and filled circles synthetic models.

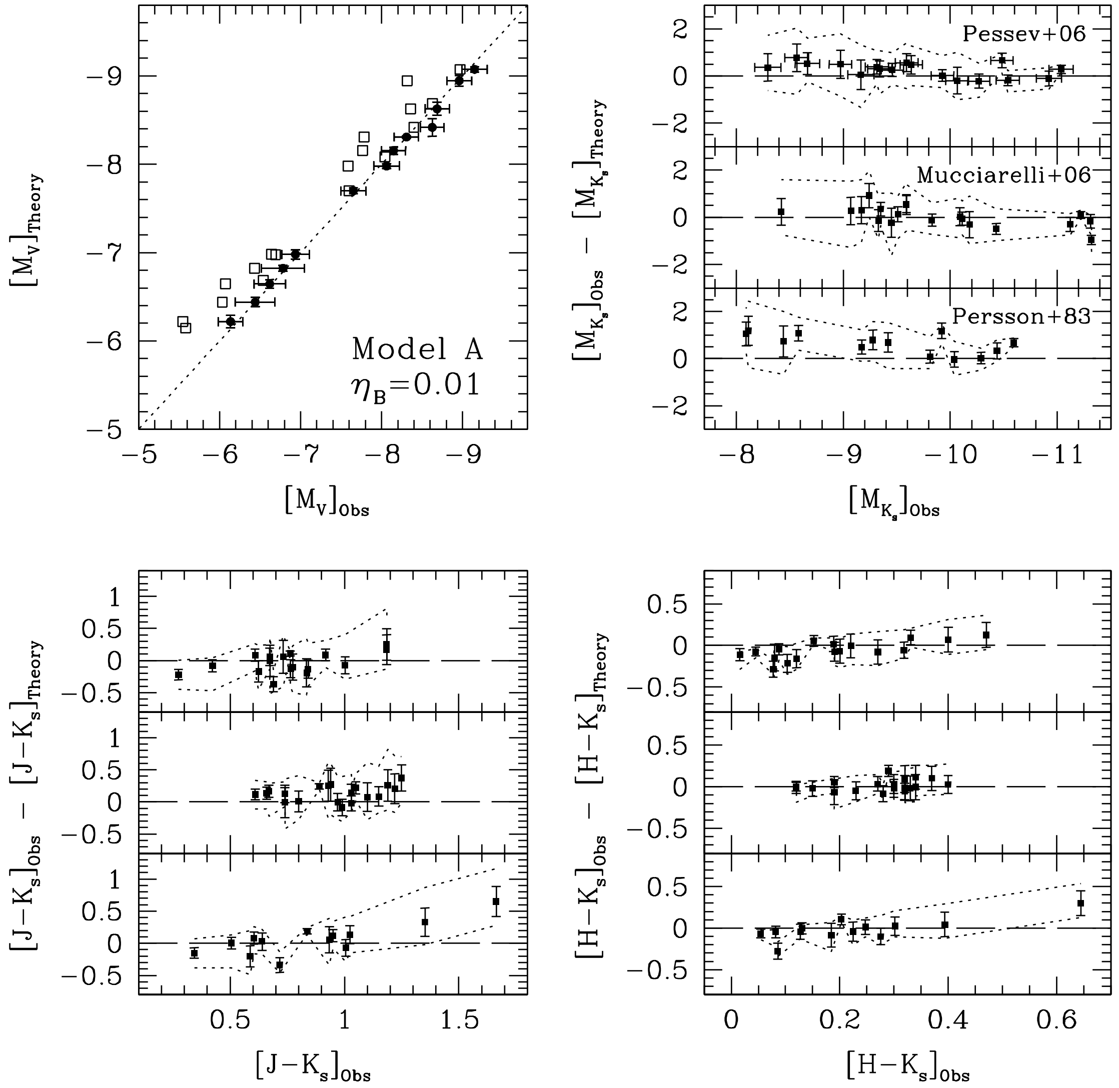

FIG. 6.— Integrated magnitudes and colors for 19 LMC clusters. Predicted values refer to *Model A*. *Upper left panel:* Predicted M_V *vs.* observed M_V of van den Bergh (1981, open squares), and Goudfrooij et al. (2006, filled circles). *Upper right panel:* The M_{K_s} magnitude difference is compared to the observed M_{K_s}. *Lower panels:* The difference between predicted and observed $J-K_s$ (left) and $H-K_s$ (right) are compared to the observed values from three different compilations: Pessev et al. (2006) (upper), Mucciarelli et al. (2006) (middle), and Persson et al. (1983) (bottom). The dotted lines mark the region covered by all the available value in the synthetic color distribution, i.e. it is related to the maximum and the minimum magnitude (color) obtained in the series of independent runs.

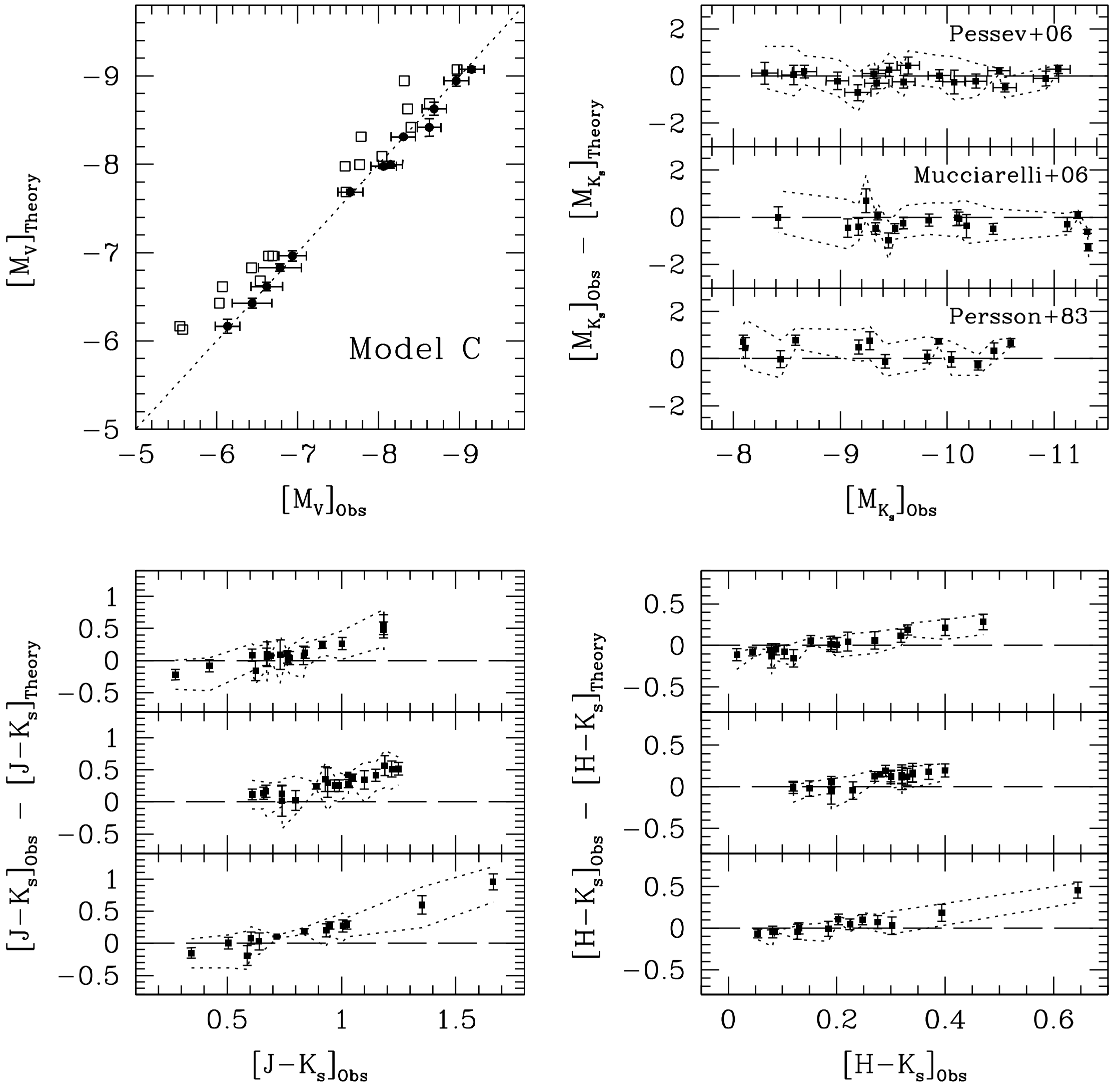

FIG. 7.— As in Figure 6, but for *Model C*.

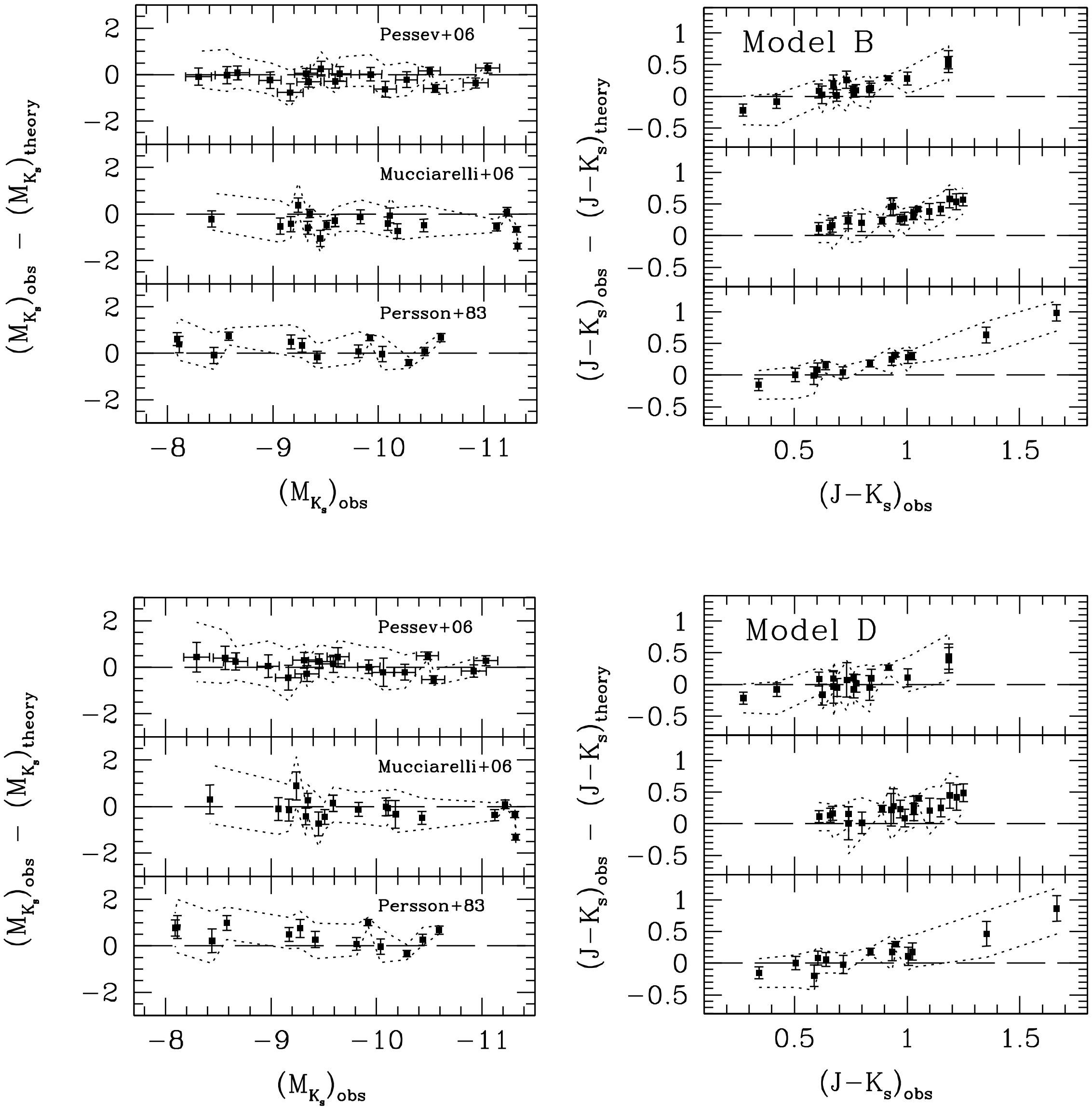

FIG. 8.— K_s-magnitude and $J - K_s$ color differences for model *Model B* (upper panels) and *Model D* (lower panel).

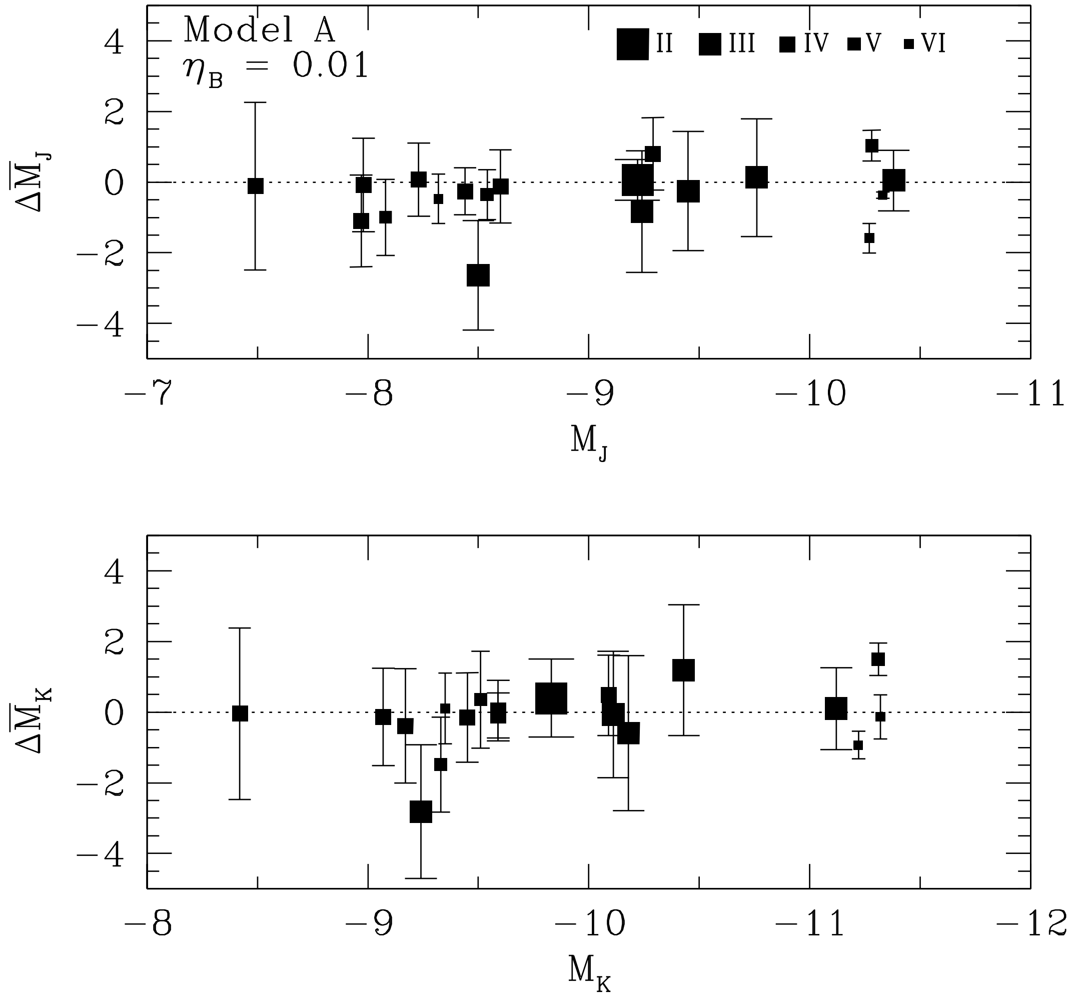

FIG. 9.— The difference between observed and predicted SBF magnitudes. Symbol size decreases from SWB class II to VI as labeled.

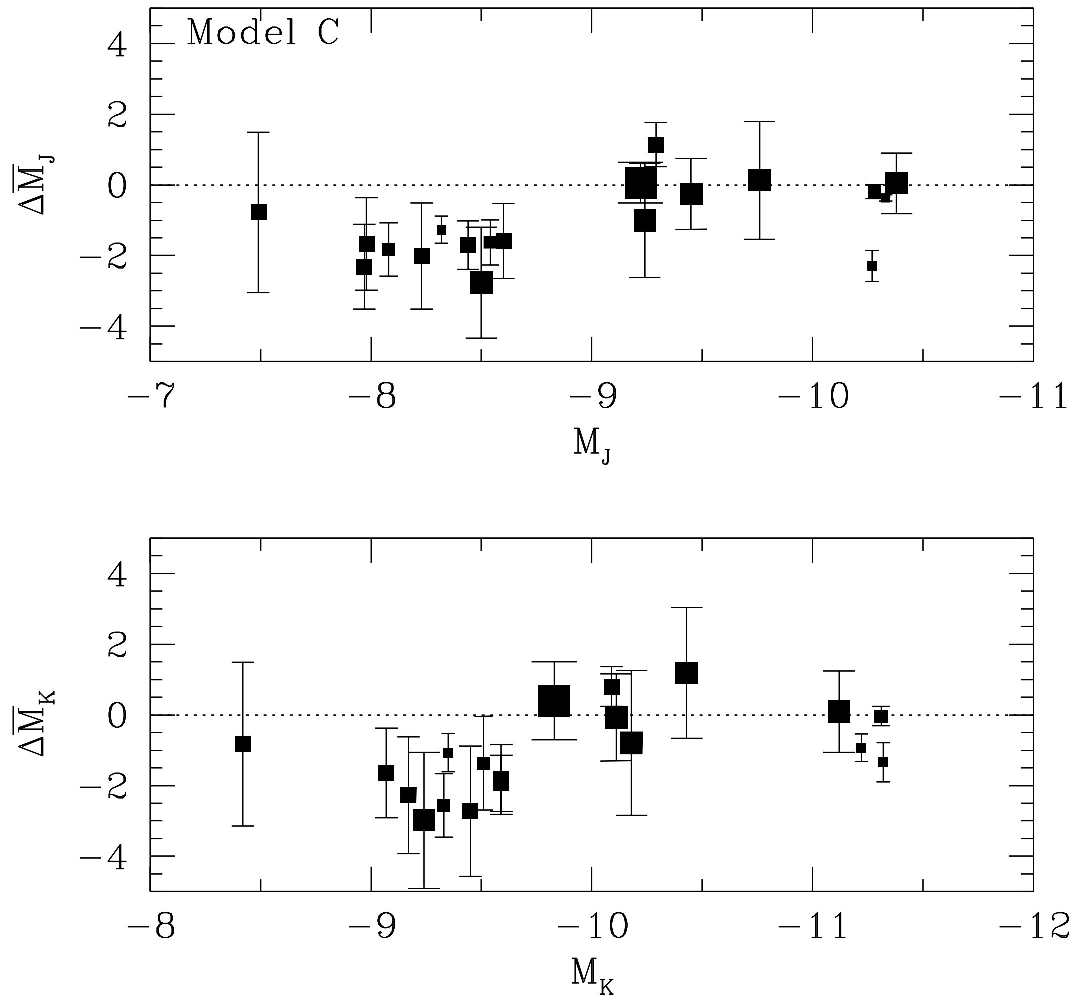

FIG. 10.— As in Figure 9, but for *Model C*.

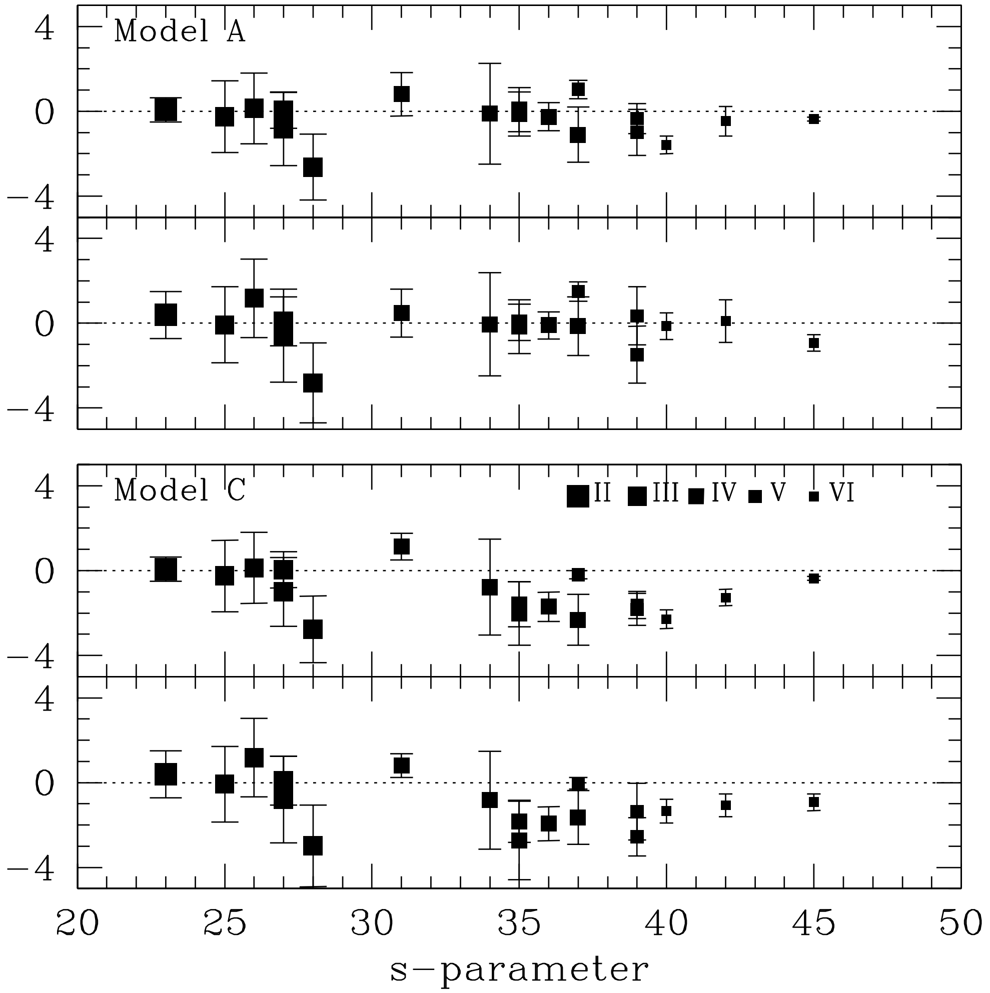

FIG. 11.— SBF-magnitude differences are plotted against the *s*-parameter.

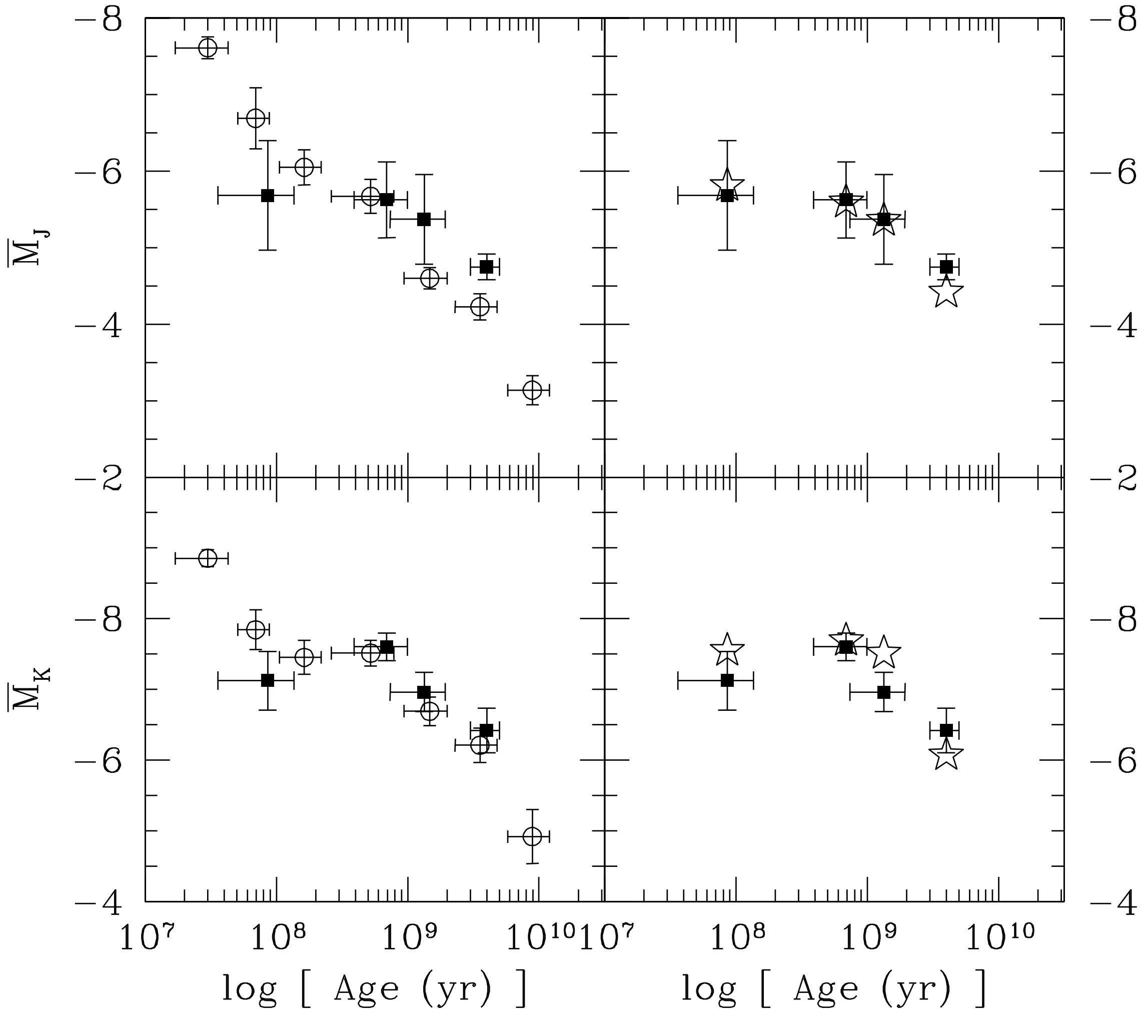

Fig. 12.— Left Panels: Observed SBF magnitudes of clusters as grouped according to Table 4 (filled squares) are compared to Superclusters' data from González et al. 2004, open circles). Right Panels: Observed SBF magnitudes of clusters as grouped according to Table 4 are compare to predictions from *model A* (open stars, see text).

TABLE 1
LMC Cluster Sample Information

Cluster Name (1)	Log Age (dex) (2)	Reference (3)	[Fe/H] (dex) (4)	Reference (5)	C-stars (Number) (6)	Reference (7)	*s* (8)
NGC 1651	$9.30^{+0.08}_{-0.10}$	5	−0.37±0.20	7	1;1;1	1;9;11	39
	9.08	1	−0.53±0.03	12			
NGC 1783	8.94	1	−0.45	8	2;4;4	1;9;11	37
NGC 1806	9.16	1	−0.23	7	4;2	1;9	40
NGC 1831	8.50±0.30	4	0.01±0.20	7	3;2	1;11	31
	8.58	1					
NGC 1866	8.12±0.30	4	−0.50±0.10	6	0;0	1;9	27
	8.20	1					
NGC 1978	9.52	1	−0.96	6	4;4;9	1;9;11	45
NGC 1987	8.79	1	−1.00	8	3;1;1	1;9;11	35
NGC 2031	8.20±0.10	2	−0.52±0.21	2	0	1	27
	8.20	1					
NGC 2108	8.86	1	−1.20	8	1;1;1	1;9;11	36
NGC 2134	8.28	1	−1.00	8	0;0	1;11	28
NGC 2136	8.00±0.10	2	−0.55±0.23	2	1;0;0	1;9;11	26
	8.13	1					
NGC 2157	7.60±0.20	3	−0.45	10	0	1	25
	8.06	1	−0.60	8			
NGC 2162	$9.11^{+0.12}_{-0.16}$	5	−0.23±0.20	7	1;0	1;11	39
	9.08	1	−0.46±0.07	12			
NGC 2164	7.70±0.20	4	−0.45	10	0	1	23
	7.91	1	−0.60	8			
NGC 2173	$9.33^{+0.07}_{-0.09}$	6	−0.24±0.20	7	1;1;1	1;9;11	42
	9.30	1	−0.42±0.03	12			
NGC 2190	8.86	1	−0.12	7	2;2	1;11	-
NGC 2209	$8.98^{+0.15}_{-0.24}$	5	−0.47	10	2;2;2	1;9;11	35
	8.79	1	−1.20	8			
NGC 2231	$9.18^{+0.10}_{-0.13}$	5	−0.67±0.20	7	1;1;1	1;9;11	37
	8.94	1	−0.52±0.03	12			
NGC 2249	8.82±0.30	4	−0.47	10	0	1	34
	8.72	1	−0.12	8			

Note. — References: (1) Mucciarelli et al. (2006), (2) Dirsch et al. (2000), (3) Elson (1991), (4) Elson & Fall (1988), (5) Geisler et al. (1997), (6) Hill et al. (2000), (7) Olszewski et al. (1991), (8) Sagar & Pandey (1989), (9) Frogel et al. (1990), (10) Mackey & Gilmore (2003), (11) Westerlund et al. (1991), (12) Grocholski et al. (2006).

TABLE 2
Synthetic properties of cluster sample

Cluster Name (1)	log Age (yr) (2)	Z (dex) (3)	M_V (mag) (4)	M_{K_s} (mag) (5)	$J-K_S$ (mag) (6)	$H-K_s$ (mag) (7)
NGC 2164	$7.70^{+0.18}_{-0.15}$	2.0e-02	−8.42±0.10	−9.7±0.3	0.49±0.09	0.12±0.05
NGC 2157	$7.72^{+0.17}_{-0.15}$	2.0e-02	−8.68±0.06	−10.0±0.3	0.52±0.11	0.13±0.07
NGC 2136	$7.72^{+0.17}_{-0.37}$	2.0e-02	−8.62±0.09	−9.9±0.3	0.50±0.11	0.14±0.07
NGC 1866	$8.08^{+0.07}_{-0.10}$	8.0e-03	−9.07±0.03	−10.8±0.3	0.61±0.15	0.17±0.09
NGC 2031	8.08±0.08	2.0e-02	−8.07±0.05	−9.9±0.6	0.67±0.28	0.22±0.16
NGC 2134	$8.18^{+0.05}_{-0.10}$	2.0e-02	−7.99±0.04	−10.2±0.6	0.75±0.25	0.25±0.15
NGC 1831	8.50±0.07	2.0e-02	−8.07±0.02	−10.1±0.4	0.79±0.18	0.28±0.11
NGC 2249	8.68±0.09	8.0e-03	−6.69±0.06	−8.7±0.6	0.68±0.26	0.22±0.14
NGC 2190	8.81±0.07	8.0e-03	−6.73±0.06	−9.5±0.6	0.93±0.26	0.33±0.15
NGC 2209	8.95±0.10	8.0e-03	−6.33±0.07	−9.2±0.7	1.01±0.25	0.34±0.15
NGC 1987	8.95±0.10	8.0e-03	−7.04±0.05	−10.1±0.4	1.08±0.14	0.37±0.10
NGC 2108	8.95±0.10	8.0e-03	−7.28±0.05	−10.1±0.5	1.06±0.17	0.37±0.11
NGC 2231	8.98±0.11	8.0e-03	−6.29±0.08	−9.3±0.6	1.02±0.24	0.34±0.15
NGC 1783	$9.08^{+0.15}_{-0.23}$	8.0e-03	−8.28±0.04	−11.1±0.3	1.05±0.13	0.36±0.10
NGC 2162	9.18±0.06	8.0e-03	−6.44±0.06	−9.2±0.5	0.88±0.22	0.27±0.14
NGC 1651	$9.23^{+0.07}_{-0.12}$	8.0e-03	−6.60±0.06	−9.6±0.4	0.97±0.15	0.32±0.11
NGC 1806	$9.34^{+0.10}_{-0.14}$	4.0e-03	−7.72±0.03	−10.4±0.2	0.83±0.11	0.23±0.09
NGC 2173	9.48±0.08	8.0e-03	−6.89±0.03	−9.7±0.3	0.89±0.15	0.26±0.11
NGC 1978	9.70±0.08	4.0e-03	−8.95±0.01	−11.3±0.2	0.65±0.05	0.10±0.07

TABLE 3
SBF MAGNITUDES OF LMC CLUSTERS

Cluster Name (1)	Models $\overline{M}_J$ (mag) (2)	Models $\overline{M}_{K_s}$ (mag) (3)	Observations $\overline{M}_J$ (mag) (4)	Observations $\overline{M}_{K_s}$ (mag) (5)
NGC 2164	-5.1 ± 0.6	-6.1 ± 0.8	-5.1 ± 0.2	-5.7 ± 0.8
NGC 2157	-5.3 ± 1.0	-6.4 ± 1.3	-5.6 ± 1.4	-6.5 ± 1.3
NGC 2136	-5.2 ± 0.7	-6.3 ± 1.0	-5.0 ± 1.5	-5.1 ± 1.6
NGC 1866	-5.5 ± 0.9	-7.0 ± 1.2	-5.5 ± 0.1	-7.0 ± 0.1
NGC 2031	-5.5 ± 1.8	-7.0 ± 2.2	-6.4 ± 0.1	-7.6 ± 0.3
NGC 2134	-5.8 ± 1.6	-7.4 ± 1.9	-8.5 ± 0.1	-10.3 ± 0.1
NGC 1831	-5.5 ± 1.0	-7.4 ± 1.2	-4.8 ± 0.3	-6.9 ± 0.1
NGC 2249	-4.5 ± 1.8	-5.9 ± 2.2	-4.6 ± 1.5	-6.0 ± 1.0
NGC 2190	-5.7 ± 1.0	-7.5 ± 1.3	-5.7 ± 0.1	-7.8 ± 0.1
NGC 2209	-5.6 ± 1.4	-7.4 ± 1.7	-5.6 ± 0.2	-7.6 ± 0.1
NGC 1987	-5.9 ± 0.5	-7.9 ± 0.6	-6.1 ± 0.9	-7.8 ± 0.6
NGC 2108	-5.9 ± 0.6	-7.8 ± 0.7	-6.2 ± 0.4	-8.0 ± 0.1
NGC 2231	-5.6 ± 1.0	-7.4 ± 1.3	-6.7 ± 0.8	-7.5 ± 0.2
NGC 1783	-5.6 ± 0.5	-7.7 ± 0.5	-4.7 ± 0.1	-6.3 ± 0.1
NGC 2162	-5.0 ± 1.0	-6.7 ± 1.4	-6.0 ± 0.4	-8.3 ± 0.6
NGC 1651	-5.3 ± 0.7	-7.2 ± 0.9	-5.7 ± 0.3	-6.9 ± 1.1
NGC 1806	-5.0 ± 0.5	-6.9 ± 0.6	-6.9 ± 0.1	-7.1 ± 0.1
NGC 2173	-4.7 ± 0.7	-6.6 ± 1.0	-5.2 ± 0.1	-6.5 ± 0.1
NGC 1978	-4.3 ± 0.1	-5.4 ± 0.1	-4.7 ± 0.1	-6.4 ± 0.4

TABLE 4
CLUSTER GROUPING AND SBF MAGNITUDES

SWB Class	s	Cluster Name	Models $\overline{M}_J$	Models $\overline{M}_{K_s}$	Observations $\overline{M}_J$	Observations $\overline{M}_{K_s}$
II	22-24	2164	...	...	...	...
III	25-29	2157,2136,1866,2031,2134	-5.8	-7.5	-5.7 ± 0.7	-7.1 ± 0.4
IV	30-36	1831,2249,1987,2209,2190,2108	-5.6	-7.7	-5.6 ± 0.5	-7.6 ± 0.2
V	37-41	2231,1806,1651,2162,1783	-5.4	-7.5	-5.4 ± 0.6	-7.0 ± 0.3
VI	42-46	2173,1978	-4.4	-6.1	-4.7 ± 0.2	-6.4 ± 0.3